Tampere University

Abdel Rahman Ez Eddin

AUTOMATIC INSPECTION OF PHOTOVOLTAIC SYSTEMS WITH THERMAL IMAGING DRONES

Faculty of Information Technology and Communication Sciences
Master of Science Thesis
Examiner: Prof. Seppo Valkealahti
November 2021

ABSTRACT

Abdel Rahman Ez Eddin: Automatic inspection of Photovoltaic systems with thermal imaging drones
Master of science Thesis, 62 pages
Tampere University
Master's Degree Program in Electrical Engineering
November 2021

Due to its economic and environmental advantages, solar photovoltaic (PV) energy has attracted significant interest in recent decades. In addition, thanks to the enormous potential of solar energy, today, photovoltaic (PV) energy is one of the fastest-growing clean energy resources. Thereby, the number of grid-connected photovoltaic (PV) systems installations is constantly growing worldwide than ever before. Commonly, solar photovoltaic (PV) power plants are comprised of hundreds or thousands of solar PV modules, which represent the main component for PV power production. However, due to various types of stresses, PV modules might be subjected to different kinds of failures and defects over their lifetime. Thus, the output power of the PV power plant might be dramatically reduced. The most common types of PV modules failures are snail trails, cracked PV cells, delamination, bypass diode failure, hot spots, EVA degradation, short-circuited sub-string, etc. Therefore, regular inspection is essential to maintain the optimal efficiency and energy yield of the PV systems.

Different techniques are used for the detection of PV modules defects and failures. The most known inspection techniques are I-V curve measurement, electroluminescence (EL) imaging, fluorescence imaging, and infrared thermography. The conventional manual inspection methods such as visual inspection and I-V curve measurement are time-consuming, inaccurate, and require significant human work. Furthermore, some of the inspection techniques are applicable only to identify specific PV module defects and are not helpful for other defects types. In recent years, the infrared thermography technique has become increasingly popular for inspection defects and failures of PV systems. This technique is fast, contactless, and cost-effective. In this technique, defective PV modules can be detected by infrared camera depending on the temperature deviations of the modules. In this respect, unmanned aerial vehicles (UAV) or drones equipped with thermal infrared imaging have become a powerful technique to detect and identify the precise location of detective cells and PV modules in PV systems. In addition, this technique can be carried out under real operating conditions of the PV system. Moreover, applying drone thermography technology for PV systems inspection saves time and reduces maintenance costs compared to the traditional inspection methods.

The main goals of this thesis are to explore and evaluate the use of aerial thermography technology to detect possible PV modules failures and defects at Tampere University Solar PV Power Research Station. This thesis was carried out in cooperation with Cleaner Future Oy. DJI Mavic 2 Enterprise Dual was used in this investigation as an inspection tool. The drone has dual infrared thermal and visual cameras. The practical measurements were carried out on 12th and 13th of May 2021. The thermographic and visual images of PV modules are captured during the measurements and subsequently extracted from DJI remote controller for further analysis. In this investigation, the achieved results showed that several defects and failures were detected by thermal drone camera, such as hot spots, EVA discoloration, and accumulation of soiling. Finally, the study results have proven that the DJI Mavic 2 Enterprise Dual with its thermal and visual cameras was helpful and reliable to identify possible failures of PV modules at Tampere University Solar PV research power station.

Keywords: Hot spot, PV module, drone, solar PV systems, defects, infrared thermal

PREFACE

This Master of Science Thesis has been achieved at the Department of Electrical Engineering of Tampere University in cooperation with Cleaner Future Oy. The company offers design and installation services of on-grid PV systems for households, farms, and industries.

The measurements have been done at Tampere University Solar PV Power Research Station, Department of Electrical Engineering. The supervisors of this thesis were Professor Seppo Valkealahti, Joni Lepistö from Cleaner Future Oy. The examiner was Kari Lappalainen.

I want to thank Professor Seppo Valkealahti for his guidance and support over the progress of completing this thesis. Great thanks to Joni Lepistö, chief executive officer of Cleaner Future Oy, for giving me this opportunity to achieve my master thesis.

I would also to thank my friend Mazin Al Qawas. Finally, I want to express my gratitude to my wife, Rahaf Al Mansour, who supported and encouraged me during difficult times.

Tampere, November 2021

Abdel Rahman Ez Eddin

CONTENTS

LIST OF SYMBOLS AND ABBREVIATIONS

SYMBOLS

E_{g}	Band gap energy
I_{ph}	Photocurrent
I_{D}	Diode current
I_{s}	Saturation current of the diode
V_{T}	Thermal voltage
m	Ideality factor
I_{sc}	Short-circuit current
V_{oc}	Open-Circuit voltage
V_{MPP}	Voltage at the maximum power point
I_{MPP}	Current at the maximum power point
P_{MPP}	Power at maximum power point
η	Efficiency of a photovoltaic cell
P_{Opt}	Optical power
E	Irradiance
A	PV cell area
AM	Air mass
FF	Fill factor

ABBREVIATIONS

BOS	Balance of system
$C0_2$	Carbon dioxide
EL	Electroluminescence
IR	Infrared radiation
IRT	Infrared thermography imaging
MPP	Maximum power point
MPPT	Maximum power point tracking
NOCT	Nominal operating cell temperature
PV	Photovoltaic
Si	Silicon
STC	Standard test conditions
UV	Ultraviolet
BIPV	Building integrated photovoltaics
UAV	Unmanned aerial vehicle
PPA	Power agreement purchase
IRT	Infrared thermography
BIPV	Building-integrated photovoltaics

1. INTRODUCTION

In recent years, it has become clear that fossil fuel-based electricity generation is not the optimal pathway for the future of power production. Moreover, due to the limitedness of gas and oil resources, their prices have risen significantly. Furthermore, burning fossil fuels such as oil, gas, and coal releases a significant amount of carbon dioxide (CO_2) emissions into the atmosphere, leading to a rise in the earth's temperature and causing global climate change. However, climate change contributes to sea-level rise, mountain glaciers melting, and severe weather conditions. Besides, the nuclear power plant disaster happened in Fukushima, Japan. This accident showed that nuclear power is not the track to follow for the future of power production. Therefore, the need for energy transition at a global level towards replacing the conventional power generation methods with clean energy resources such as photovoltaics, wind power, and biomass represents the pathway for greenhouse gas emissions mitigation. Nowadays, due to the great potential of the sun, solar photovoltaic energy is one of the most promising clean energy resources. Photovoltaic (PV) technology converts sunlight directly into electrical energy, and it does not produce carbon dioxide (CO_2) emissions into the atmosphere [1].

Solar PV energy can cover a variety of power applications such as small-scale residential PV systems, commercial PV systems, Building-integrated Photovoltaics (BIPV) solutions, PV systems for agriculture greenhouses, and large utility-scale PV power plants. As shown in figure 1.1, in 2020, the share of installed solar PV capacity has reached 38% of all new power generation installations.

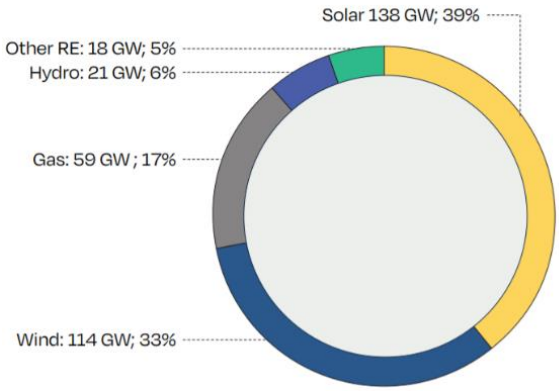

Figure 1.1. *Net installed power generation capacity added in 2020* ***[2]***

The solar PV market is expected to grow strongly over the coming years as seen in figure 1.2. According to the latest report published by Solar Power Europe regarding the global solar PV market, over the coming years, the global installed solar PV capacity portfolio is expected to increase in the medium scenario to 1.6 TW by 2024 [2].

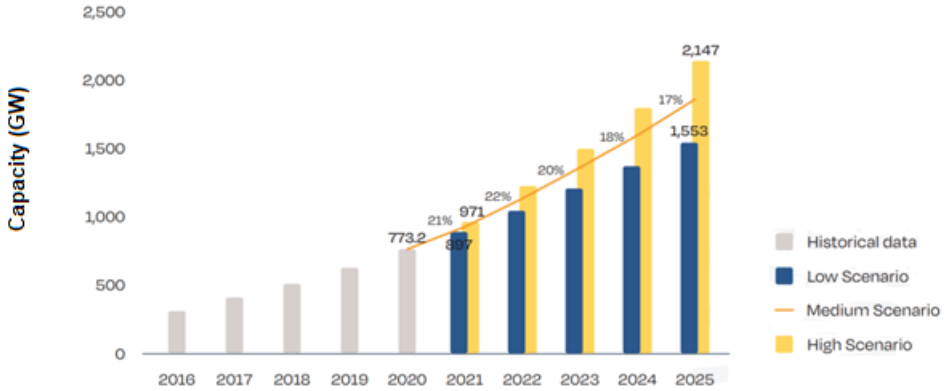

Figure 1.2. *The installed new PV generation capacity added each year with a forecast until 2025* ***[2]****.*

The output power of solar PV power plants and their payback periods are crucially dependent on the electrical performance of the PV modules and their operational lifetime. Moreover, the long-run performance and reliability of PV modules can be significantly influenced by failures and defects occurring during the transportation, installation, and under real operation conditions. Thus, these faults might lead to abnormal operation and reduction of the power generation of the PV system, in addition to abnormalities in the thermal profiles of PV modules. However, detection of PV modules faults under normal operating conditions for large-scale solar PV power plants, with thousands of PV modules, represents an operational and economic challenge. The traditional inspection method of PV modules using *I-V* curve measurements has limited capability for detecting defects and failures. In this method, the physical fault location can be determined only by performing the electrical measurements on the PV module level. Thus, in practice, such a method cannot be appropriate or acceptable by PV power plants operators because it is time-consuming and not economically viable. Electroluminescence (EL) is a good tool for inspecting PV cells micro-cracks, broken contacts, or failures in the antireflection coating. EL imaging test is usually done at nighttime or after the PV system operation is interrupted. In this method, the inspection process is performed on PV modules one by one. Thus, Electroluminescence (EL) might not be practicable for inspecting large-scale PV systems. Nowadays, advanced inspection method based on infrared thermography has become more popular. In this technique, a thermal camera can detect

and localize defective cells and modules through their temperature profiles. Drones with a thermal imaging camera, sometimes called aerial thermography, offer speed and accuracy that is many times higher than traditional inspection methods. With this technique, the balance of system (BOS) components such as cables, fuses, combiner boxes, etc., may be tested for temperature abnormalities [3] [4].

The thesis concern is about the automatic inspection of Tampere University solar PV research power station using thermal imaging drone technology. In this thesis, the measurements were carried out by DJI Mavic 2 Enterprise Dual, on 12th and 13th of May 2021. Several factors were carefully considered during the measurements process for achieving reliable and accurate results. Thus, the measurements were implemented during sunny days with low wind speed and sufficient solar radiation. Captured thermal images information has been analyzed to define whether the PV modules in the research PV power plant have possible failures or defects.

The structure of this thesis starts as follows: Chapter 2 gives a brief theory about the basics of photovoltaic (PV) technology. The fundamentals of photovoltaic cells, PV modules, PV generator, temperature and irradiance effect, and grid-connected PV systems are presented. Chapter 3 displays the common failures and defects modes of the PV modules. These failures and defects include hot spots, PV cells cracks, snail trails, EVA discoloration, delamination, and broken interconnects. After that, an overview of existing photovoltaic (PV) inspection methods are illustrated in chapter 4. It includes visual inspection, *I-V* curve measurement, electroluminescence (EL), infrared thermography. Chapter 5 deals with the practical details related to the measurements process, the results, and the analysis. In this chapter DJI Mavic 2 Enterprise Dual, Tampere University solar PV power research station, implementing the flight mission, and case studies are discussed and analyzed in detail. Finally, the conclusion and limitations are illustrated in chapter 6.

2. PHOTOVOLTAIC TECHNOLOGY OVERVIEW

In this chapter, the basics and background of photovoltaic cells, PV modules, PV generators, temperature and irradiance effect on PV modules performance, and grid-connected PV systems are briefly discussed.

2.1 Photovoltaic cells

Photovoltaics (PV) is the process of converting sunlight directly into electricity using PV cells. The term photovoltaics comes from combining two words, the Greek word photo, meaning light, and the word volt derived from the name of the Italian physicist Alessandro Volta, referring to the unit of voltage. Alessandro Volta invented the first functional electrochemistry battery. Figure 2.1 shows the PV cell structure and PV cells as the main component of the PV module [1].

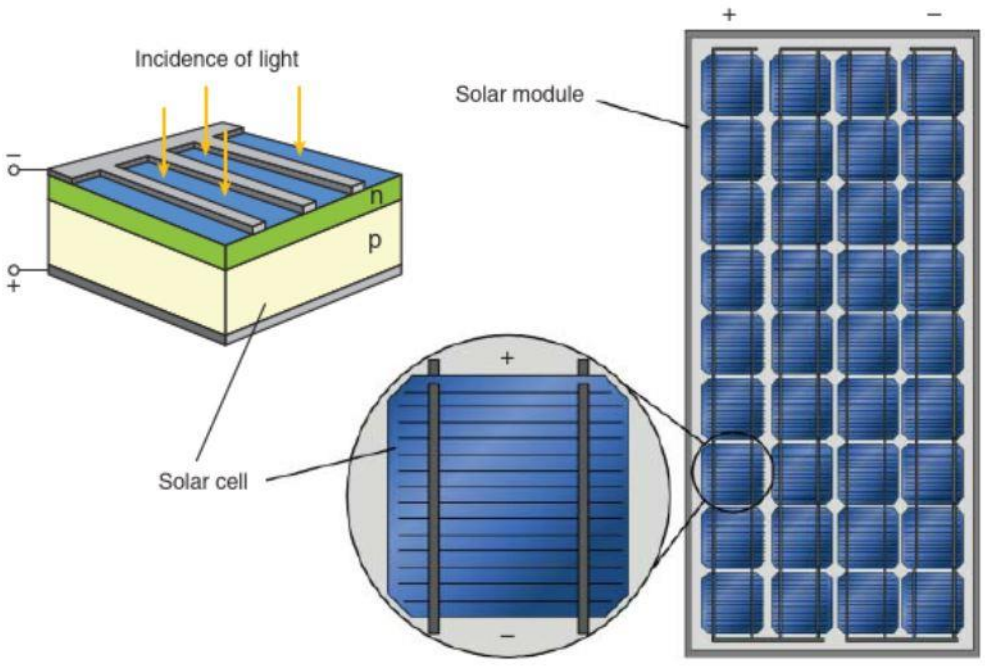

Figure 2.1. *Structure of a PV cell and PV module as main components of PV systems* ***[1]****.*

PV cells are the building blocks of PV power plants, which are made of semiconductor materials. In most cases, PV cells are based on silicon (Si). Furthermore, intrinsic semiconductors are doped with impurities, where holes and electrons are injected by a foreign atom to achieve p-type semiconductor and n-type semiconductor, respectively. Thus, a

p-n junction is formed when p-type and n-type layers are joined together, and an electric field is created at the p-n junction. When the light strikes the PV cell with sufficient photon energy, electrons can be moved out from the valence band into the conduction band. The minimum energy needed to excite an electron from the valence band to the conduction band is known as band gap energy E_g. Thus, the charge carriers are moved by an electric field into the metallic contacts of the PV cell and generate a voltage of 0.5V across the p-n junction. The current generated by PV cells is dependent on the area of PV cells and solar radiation, which can vary from 0 to 10 A [1] [5].

2.1.1 Working principle of photovoltaic cells

Silicon PV cells are composed of two semiconductor layers, a p-type, and an n-type layer. Therefore, the p-n junction is created by joining the p-type and n-type layers together. Furthermore, the top side of the PV cell is a highly doped n^+-type, and the p-type is on the bottom side. When sunlight hits the PV cell, the absorption of the photons generates an electron-hole pair, where the electrons and holes are separated from the depletion region and transferred to n-type and p-type layers, respectively. Moreover, the generated electrons are gathered through PV cell grid lines and transported to the PV cell busbars. Thus, an electric current is generated if an external load is connected to the PV cell. Figure 2.2 illustrates the structure of typical silicon PV cell [1].

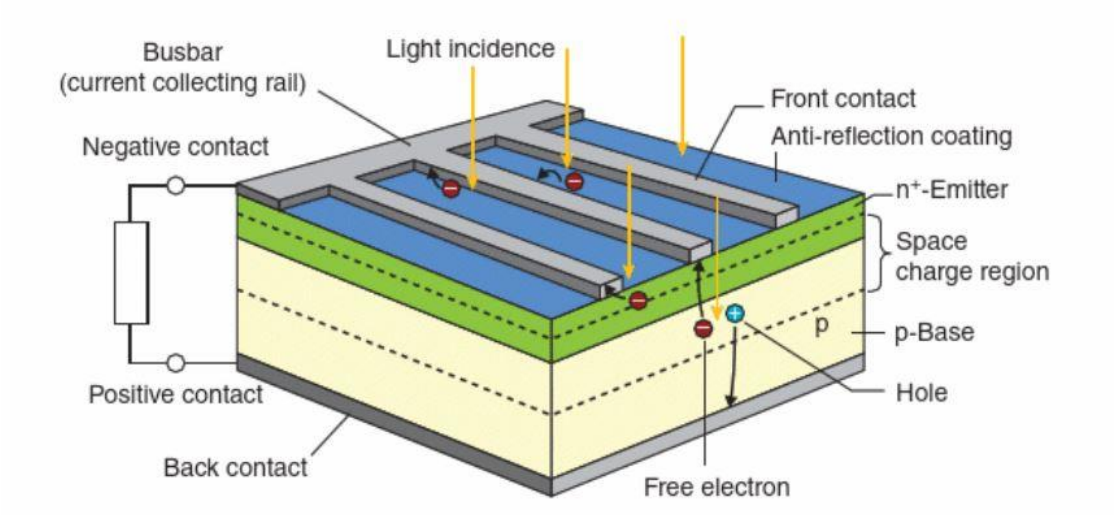

Figure 2.2. *Typical Silicon PV cell structure* ***[1]****.*

2.1.2 Current-voltage characteristics of photovoltaic cells

Figure 2.3 below illustrates the current-voltage *(I-V)* characteristic curve of a typical PV cell in addition to its simplified equivalent circuit.

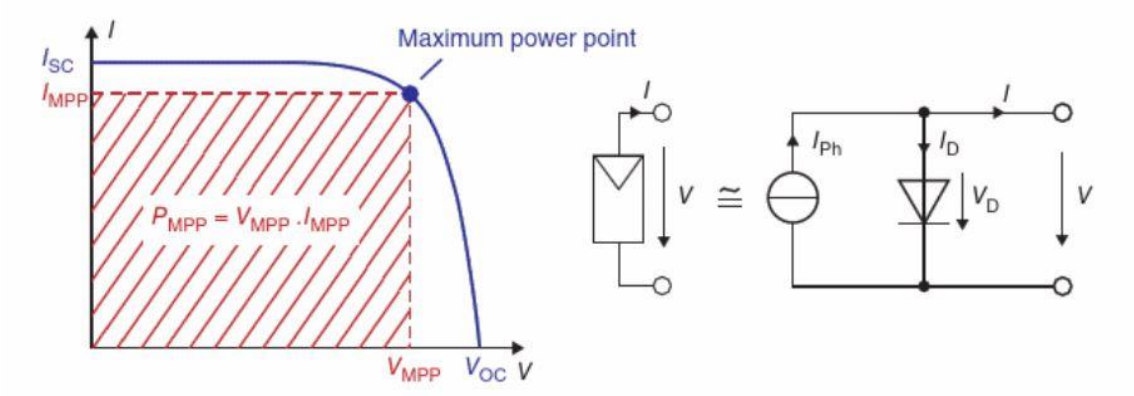

Figure 2.3. *I-V characteristics curve and simplified circuit of PV cell* ***[1]****.*

The I-V curve equation can be expressed as follows:

$$I = I_{\text{ph}} - I_D = I_{\text{ph}} - I_s\left(e^{\frac{V}{m.V_T}} - 1\right) \quad (1)$$

Where, I_{ph} is the photocurrent, I_s the saturation current of the diode, V_{T} the thermal voltage, *v* the voltage is applied to the device, and *m* the ideality factor. One of the main parameters of the PV cell is the ideality factor *m*. The value of the ideality factor can vary between 1 and 2.

Several PV cell parameters are introduced from the *I-V* curve characteristic, which is illustrated in figure 2.3. The short-circuit current I_{sc} is the current produced by the PV cell when its terminals are short-circuited. Thus, the PV cell voltage in this case is zero. The second parameter is open-circuit voltage V_{oc}, which takes place when the current of the PV cell is zero. Maximum power point (MPP) represents the operating point of the PV cell when the power generated is maximum from the PV cell. However, depending on where the actual PV cell operating point is operated, PV cell may produce different range of powers. Furthermore, MPP power is the product of the corresponding maximum power point current I_{MPP} and voltage V_{MPP}. The fill factor (*FF*) represents the ratio of the area defined by product of V_{MPP} and I_{MPP} divided by the product of V_{oc} and I_{sc}.

$$FF = \frac{V_{\text{MPP}}.I_{\text{MPP}}}{V_{\text{oc}}.I_{\text{sc}}} \quad (2)$$

where, V_{MPP} is the voltage at maximum power point, I_{MPP} is the current at the maximum power point, V_{oc} is the open-circuit voltage, and I_{sc} is the short-circuit current. Typical *FF*

values may range between 0.75 and 0.85 for silicon PV cells, and between 0.6 and 0.75 for thin-film PV cells. *FF* is an indicator of PV cell quality. Current-voltage curve, power-voltage curve, and fill factor are illustrated in figure 2.4.

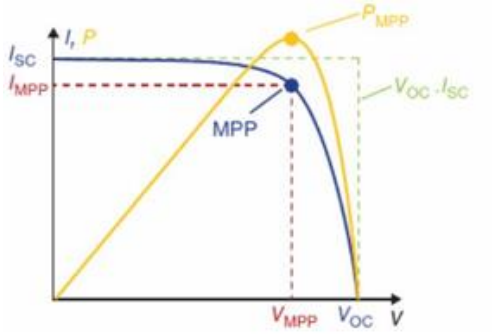

Figure 2.4. *Power-voltage curve, current-voltage curve, and fill factor* ***[1]****.*

PV cell efficiency refers to the ratio of the power output of the PV cell to the incident energy of the sun on the PV cell surface.

$$\eta = \frac{P_{\mathrm{MPP}}}{P_{\mathrm{Opt}}} = \frac{P_{\mathrm{MPP}}}{E.A} = \frac{FF.V_{oc}.I_{sc}}{E.A} \tag{3}$$

Where, *A* indicates to the PV cell area, P_{opt} is the optical power, P_{MPP} is the power at the maximum power point, *E* is the irradiance, V_{oc} is the open-circuit voltage, and I_{sc} is the short-circuit current. According to the latest report published by National Renewable Energy Laboratory (NREL), for crystalline silicon PV cells, the efficiency may range between 21.2% and 27.6% depending on cell type, as shown in figure 2.5 [1] [6].

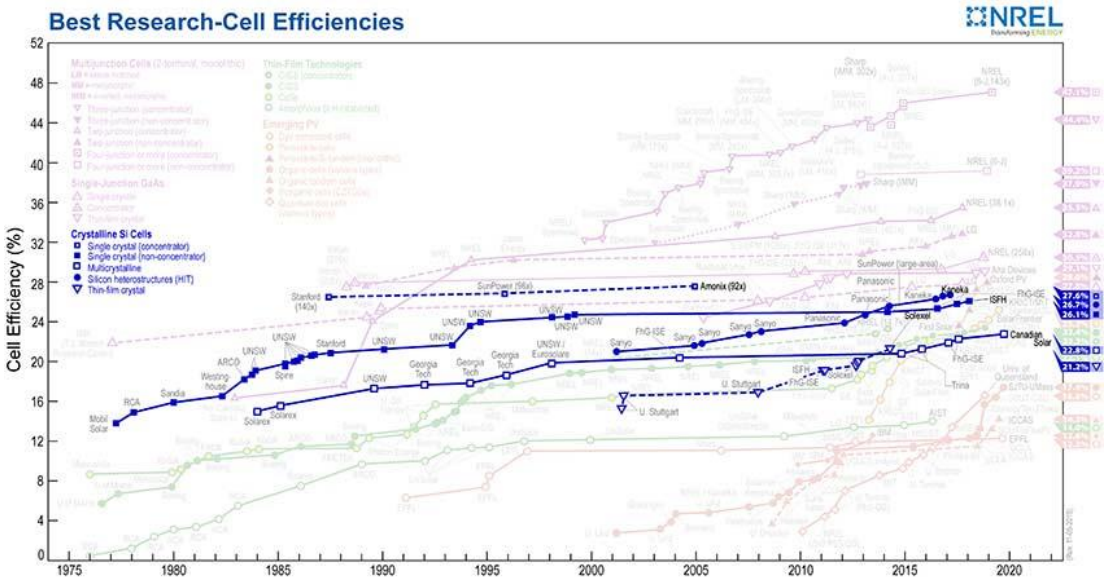

Figure 2.5. *Silicon PV cell efficiency record from 1975 to 2020* ***[6]****.*

2.2 Photovoltaic modules

The open-circuit voltage produced by silicon solar cells is very low which can vary from 0.55 to 0.72 V at Standard Test Conditions (STC), while the voltage at the maximum power point V_{MPP} is about from 0.45 to 0.58 V. Therefore, solar PV cells voltage is insufficient for practical applications. Thus, a higher voltage can be obtained by connecting multiple solar cells in series to make it suitable for PV system operation. Solar PV modules can be formed by connecting several PV cells in series which range from about 32 to 72 solar cells and to protect them against the environmental impacts, the solar cells are placed in a single framework.

For 12 V stand-alone PV systems consist of one PV module and battery. PV modules that consist of 36 PV cells are commonly used with operating voltages from 15 to 20 V and power output varying from 50 to 200 Wp. Furthermore, for 24 V stand-alone PV systems, PV modules of 72 cells are appropriate choice with operating voltages varying from 30 to 40 V. Figure 2.6 shows typical layout of PV module consisting of 72 polycrystalline silicon solar cells with peak output power of 175 Wp.

Figure 2.6. *PV module with 72 polycrystalline PV cells* ***[5]****.*

Some of manufacturers indicate that the lifetime of PV modules is about 30 years, with a power output guaranteed from 10 to 26 years. However, PV modules under real operating conditions are subjected to environmental influences. Therefore, the lifetime of PV modules is mainly dependent on how capable they are to resist the ambient influences. PV module glass should be tempered and has low iron to provide high transparency of the sunlight. Plastic polymer material such as ethylene-vinyl-acetate (EVA) is commonly used to encapsulant the PV cells within two layers. Depending on the manufacturer, the back layer can be made of a glass plate or plastic sheet. Additionally, a frame surrounding the entire PV module is needed to provide mechanical stability and a protection layer. The metal frame is usually made of aluminum [5].

2.3 Photovoltaic array

When the amount of the electrical power generated by a single PV module is insufficient to supply power for a specific application, multiple PV modules are electrically connected to form a PV array. When PV modules are connected in series, higher voltages are achieved while the current remains the same as it would be for a single PV module current. When PV modules are connected in parallel, a higher current is, while the voltage remains the same as it would be for a single PV module voltage. PV array output peak power can range from some hundred watts to several megawatts. Furthermore, large-scale PV systems are usually formed by splitting the PV array into independent subarrays that are connected to balance of system (BOS). PV systems can be installed in different ways, such as a rooftop, pole-mounted or racking PV system. Rooftop PV systems are commonly used for on-grid PV systems, whereas pole-mounted PV arrays might be used for off-grid PV systems [7] [8].

A PV string is created by connecting PV modules in series. Only the PV modules with identical electrical specifications and the same type should be connected. PV modules are equipped with bypass diodes, and depending on the manufacturers generally, it can vary from 2 to 6 diodes. When a PV system includes more than three PV strings, a fuse must be added on string level to provide short circuit protection against the reverse current [5].

As shown in figure 2.7, to achieve the desired PV system voltage, PV generators are usually built by connecting PV modules in series to form PV strings. PV strings are then connected in parallel to achieve a higher current. PV strings should have the same voltage. Strings with different voltages lead to mismatch and cause a reduction in the total PV output power [5].

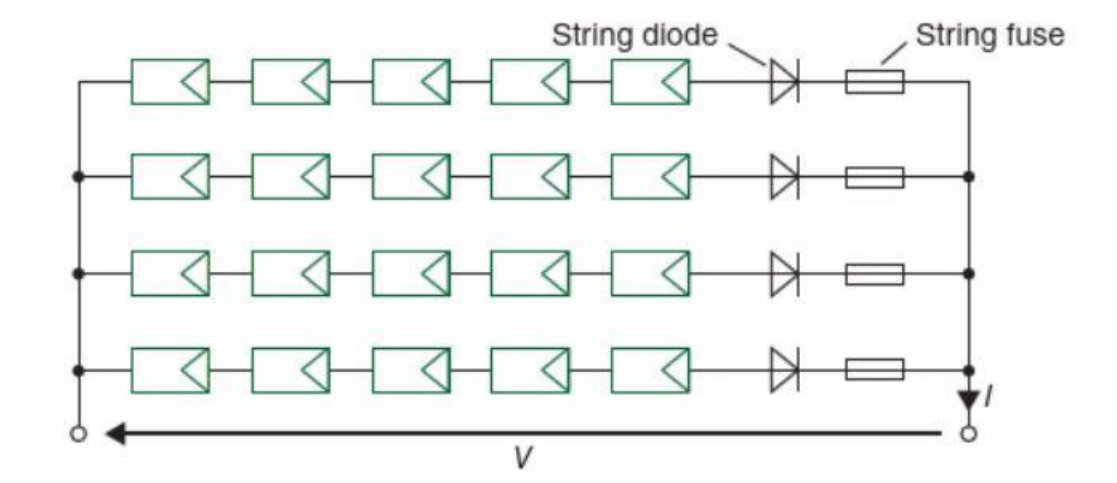

***Figure 2.7**. Structure of PV generator with multiple strings connected in parallel **[1]**.*

2.4 Effect of temperature and irradiance on photovoltaic cell operation

The performance of photovoltaic cells and modules is strongly affected by environmental conditions. Solar irradiance and temperature of the PV cell have a direct impact on the power output. Moreover, many factors may influence the temperature of the PV cells, such as wind speed, the intensity of incident solar radiation, and ambient temperature, in addition to the physical structure of the PV cells. Furthermore, the manufacturers provide the electrical characteristics of PV modules under standard test conditions (STC), which refer to solar radiation of $1000\ \mathrm{W/m^2}$, PV cell temperature of 25 ℃, and solar spectrum of air mass AM 1.5. However, in real life, standard test conditions (STC) rarely happen. Thus, for more realistic conditions, the temperature of the PV module is defined under nominal operating cell temperature (NOCT) conditions. These conditions specify a solar irradiance of $800\ \mathrm{W/m^2}$, ambient temperature of 20 ℃, solar spectrum AM 1.5, and wind speed of $1\ \mathrm{m/s}$ [9] [10].

2.4.1 Temperature effect

PV cell operating temperature plays an essential role in the conversion process of photovoltaic energy. Figure 2.8 shows the *I-V* curve of the PV cell at three different operating temperatures. It can be noticed from figure 2.8 the short-circuit current increases slightly with increasing the operating temperature of the PV cell, and the open-circuit voltage decreases significantly as the operating temperature increases. Decreasing open-circuit voltage with the temperature increase is attributed to the decrease in the band gap energy of the semiconductor. For the silicon PV cells, the temperature coefficient of the open-circuit voltage V_{oc} is about $-2.3\,\mathrm{mV/°C}$. Thus, the open-circuit voltage decreases with increasing the temperature by $2.3\,\mathrm{mV/°C}$. On the other hand, the PV cell generates higher voltage and power when its temperature decreases. Furthermore, the increase of short-circuit current at high temperatures is insignificant compared to the decrease in open-circuit voltage values. Thereby, the main effect of the operating temperature of the PV cells is mainly on the open-circuit voltage [9].

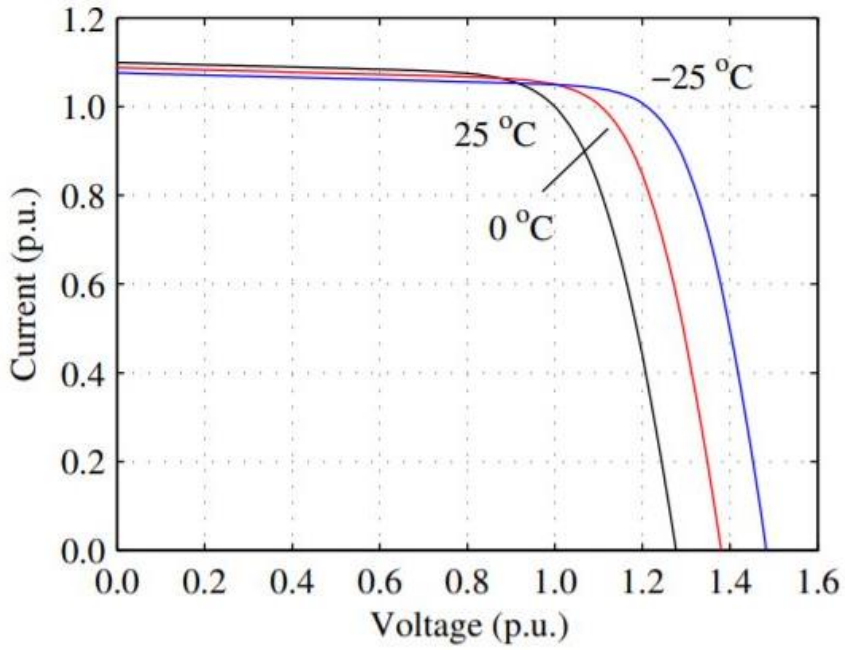

Figure 2.8. *PV cell I-V curve for different operating cell temperatures with irradiance of 1000* $\boldsymbol{W/m^2}$ ***[9]****.*

Figure 2.9 shows the open-circuit voltage, the short-circuit current, and the output power of the PV cell as a function of the operating temperature. As can be noticed from figure 2.9, an increase in the temperature of the PV cell tends to slightly increase the short-circuit current while significantly decrease the open-circuit voltage. Thus, the output

power of the PV cell decreases since the voltage decrease is more than the current increase [10].

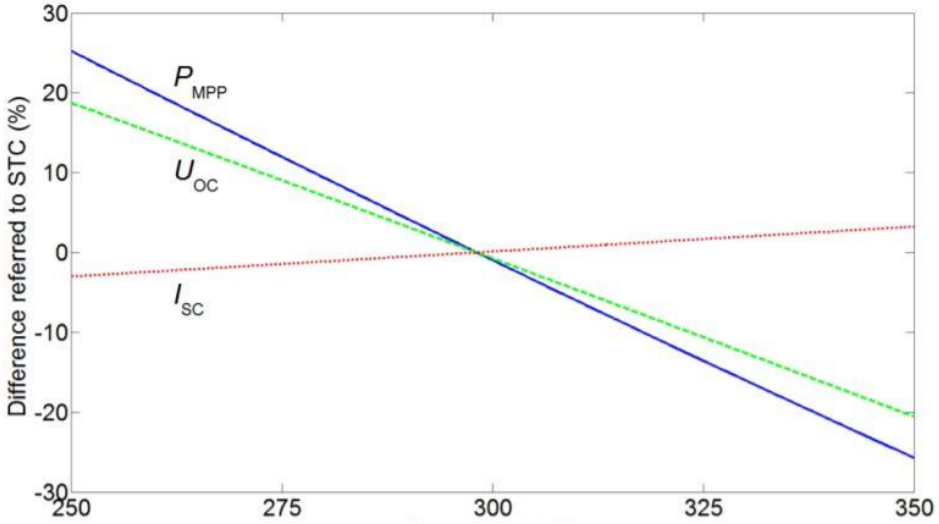

Figure 2.9. *Open-circuit voltage, Short-circuit current and output power of the PV cell as a function of temperature* ***[10]****.*

2.4.2 Irradiance effect

Figure 2.10 illustrates the *I-V* characteristic curve of the PV cell at different irradiance levels. As can be seen from figure 2.10 that the short-circuit current is directly dependent on the incident irradiance level. Thus, the short-circuit current increases proportionately

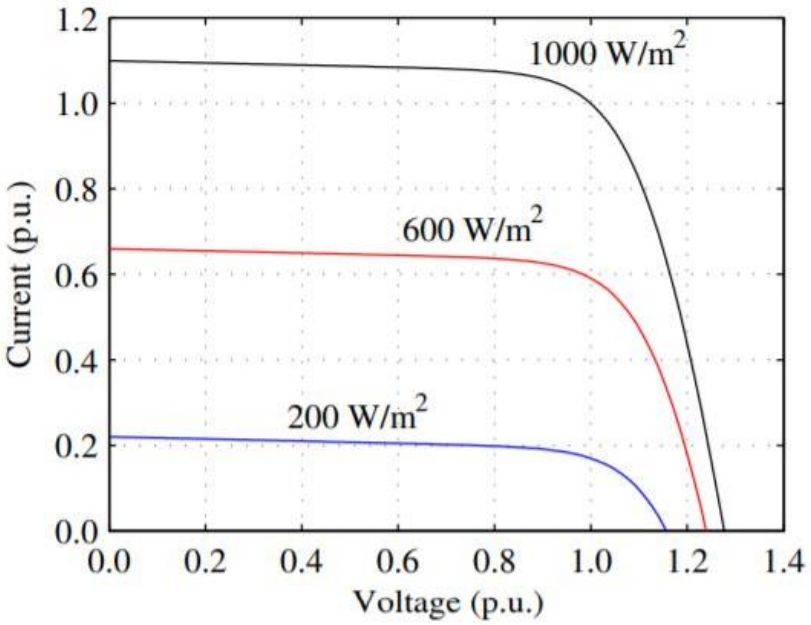

Figure 2.10. *Characteristics I-V curves of PV cell at different irradiance levels* ***[9]****.*

as the irradiance level increases, while the open-circuit voltage increases slightly with increasing the irradiance level [9].

The open-circuit voltage, the short-circuit current, and the maximum power output of the PV cell as a function of irradiance is illustrated in figure 2.11. As can be observed, the short-circuit current and the maximum power output increase dramatically with increasing the irradiance level, whereas the open-circuit voltage increases marginally as the irradiance increases [10].

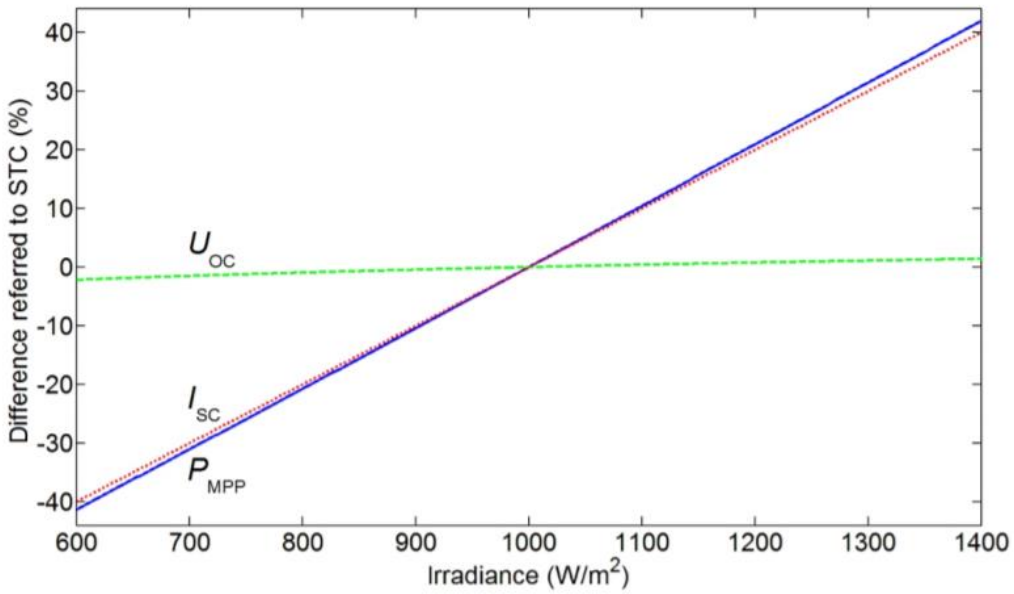

Figure 2.11. *The open-circuit voltage, the short-circuit current and the maximum power of the PV cell as a function of the irradiance* ***[10]****.*

2.5 Grid-connected photovoltaic systems

A grid-connected PV system is a PV generator that is designed to interface to the electricity grid. It exists in areas where the power grid is accessible. Grid-connected PV systems may supply power to commercial buildings and properties, and the surplus electricity generated by the PV system can be fed back into the electrical grid. Thus, the property owner will be paid for the exported power to the grid. In these systems, when the produced PV power is not sufficient to meet the energy demand of the building, the power can be drawn from the power grid. However, depending on the needs of the owner property, grid-connected PV system size may vary from small-scale to large-scale PV systems. Batteries are used in the off-grid PV systems to store the power generated by PV modules, whereas in the grid-connected PV systems, the electrical grid can be seen as a large storage device [12].

The main components of grid-connected PV systems are the PV modules and the inverters. The DC power is generated by PV modules, then DC voltage will be boosted by DC/DC converter and converted to AC power via an inverter. This AC power is further supplied into the electricity grid. DC/DC boost converter is a maximum power point tracking (MPPT) technique used to maximize the DC power generated by PV modules. Figure 2.12 shows the block diagram of the grid-connected PV system.

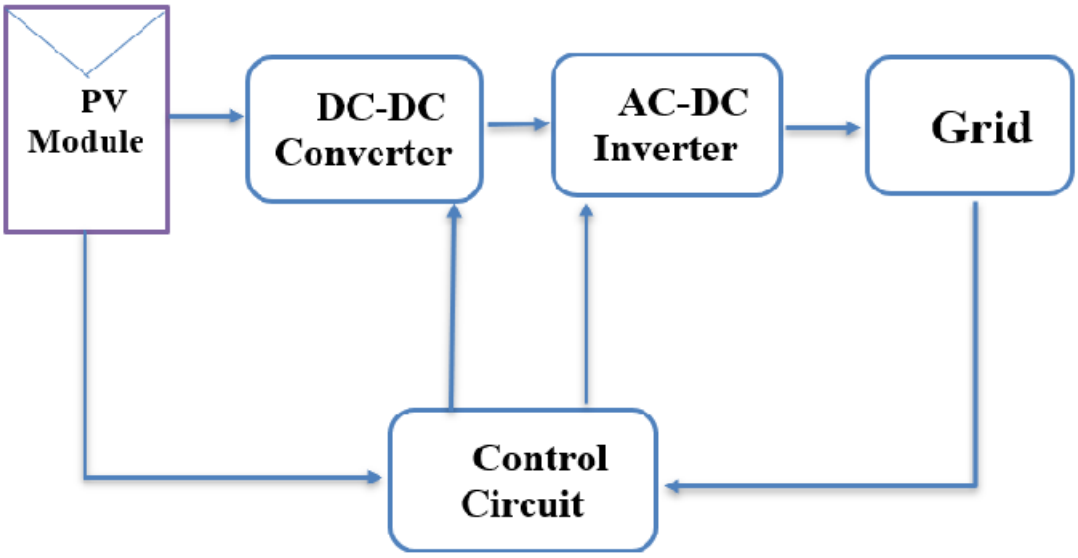

Figure 2.12. *Block diagram of grid-connected PV system* ***[13]****.*

Depending on the type of the inverter, a grid-connected PV system can be configured in four main topologies. A Centralized inverter, multi-string inverter, string inverter, and AC-module inverter may be applied.

Centralized inverters are usually applied for large-scale PV power plants, where the PV system includes a centralized inverter with one common MPPT for PV array. In addition, the PV array is built by connecting PV modules in series to form PV strings to achieve the desired voltage, and PV strings are then connected in parallel to achieve the needed current. Thus, higher power is obtained by a series-parallel connection of PV modules. Centralized inverters offer the possibility to build PV systems with much higher rated power up to several megawatts. However, Centralized inverters have some drawbacks due to the centralized MPPT. In this topology, mismatch losses occur when the PV modules are subjected to different operating conditions due to partial shading. Hence, the system efficiency decreases, and the PV power output gets drops. Besides, high DC

voltage cables are needed between the centralized inverter and PV array. Figure 2.13a shows centralized grid-connected inverter-based topology.

As a result of centralized inverter drawbacks, more development led to introduce multi-string and string inverter topologies. As shown in Figure 2.13b, the string inverter system is formed by connecting a PV string that consists of a specific number of series-connected PV modules to the inverter, which supplies the AC power into the grid. In this topology, each PV string is connected to its own MPPT. Therefore, the mismatch losses between the PV strings reduce, and energy harvesting is better than the centralized system. However, the power range of string inverters is low up to 5 KW due to the limitation of connecting PV modules in series. Therefore, to overcome the limited power of string inverter topology, a new concept called a multi-string inverter is developed.

As shown in Figure 2.13c, multi-string inverter topology consists of multiple DC/DC converters where each PV string is connected to its own DC/DC converter with separate MPPTs. Then the AC power is fed into the grid by a common DC/AC inverter. The main advantages of multi-string inverters compared to centralized inverters are more flexibility in the design of the PV systems, reliability, and increasing the efficiency of the system. Furthermore, multi-string inverter topology enables the PV system expansion by adding new PV strings to their MPPT.

Microinverter topology enables the integration of the PV module and the inverter into a consolidated system where each PV module is connected to a small size, low-rated power inverter, and individual MPPT. The power is then fed into the AC grid directly by the microinverter. In this topology, the mismatch losses between PV modules are removed. Figure 2.13d shows the microinverter topology [13].

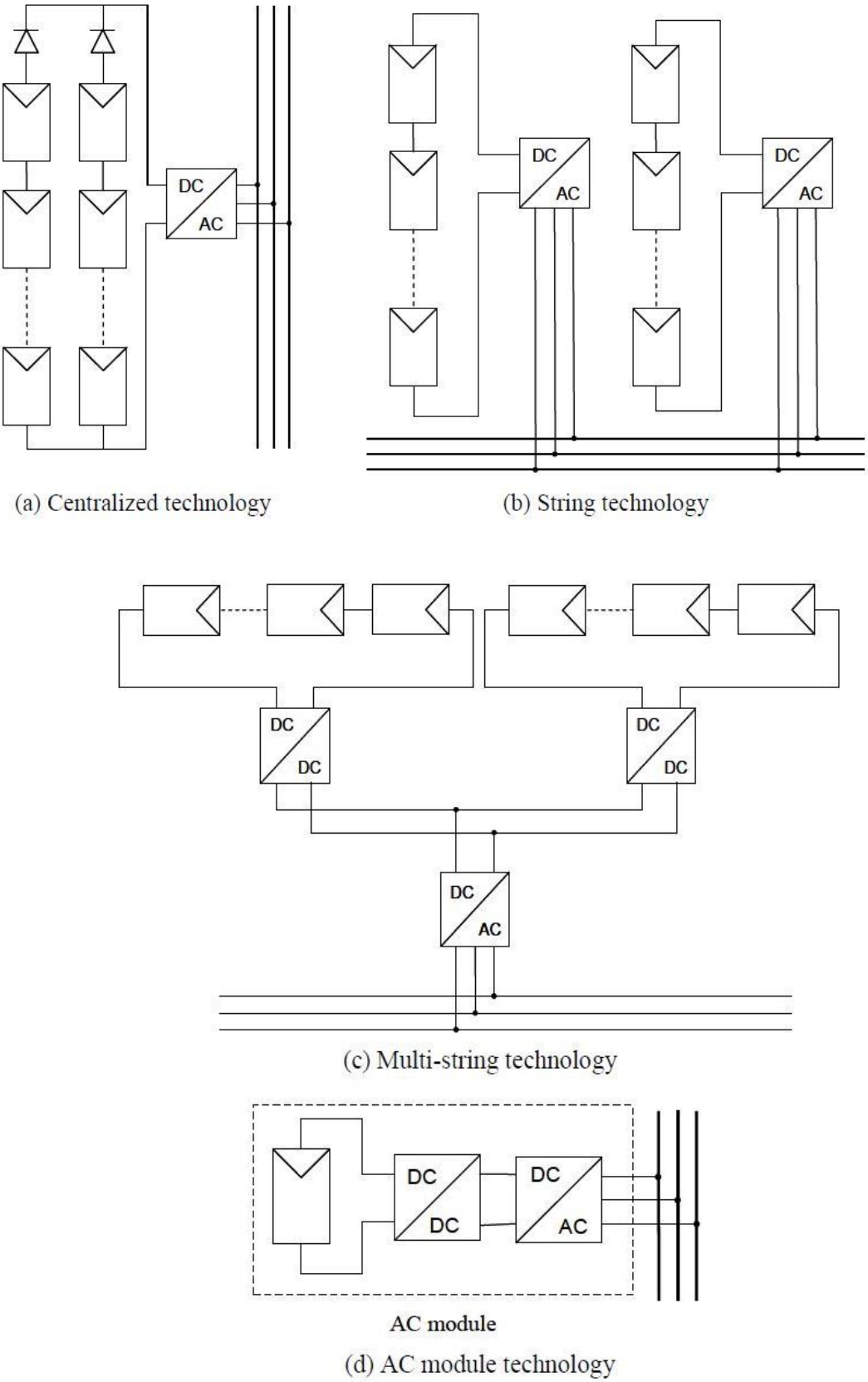

Figure 2.13. *Gid-connected PV system topologies* ***[13]***.

3. PHOTOVOLTAIC MODULES FAILURE MODES

Since PV modules operate in the outdoor environment, their materials are exposed to loads that can affect the performance of PV modules and lead to degradation impacts. These loads can be classified into external loads which result from the weather conditions and internal loads, which might be related to the PV module operation itself. However, PV module degradation is essentially impacted by the external loads. As illustrated in figure 3.1, these loads are temperature, humidity, wind, snow, ultraviolet (UV) radiation, in addition to chemical and biological loads [14].

PV modules failures such as hot spots, cells cracks, snail trails, encapsulant discoloration, delamination and broken interconnects are briefly discussed in this chapter.

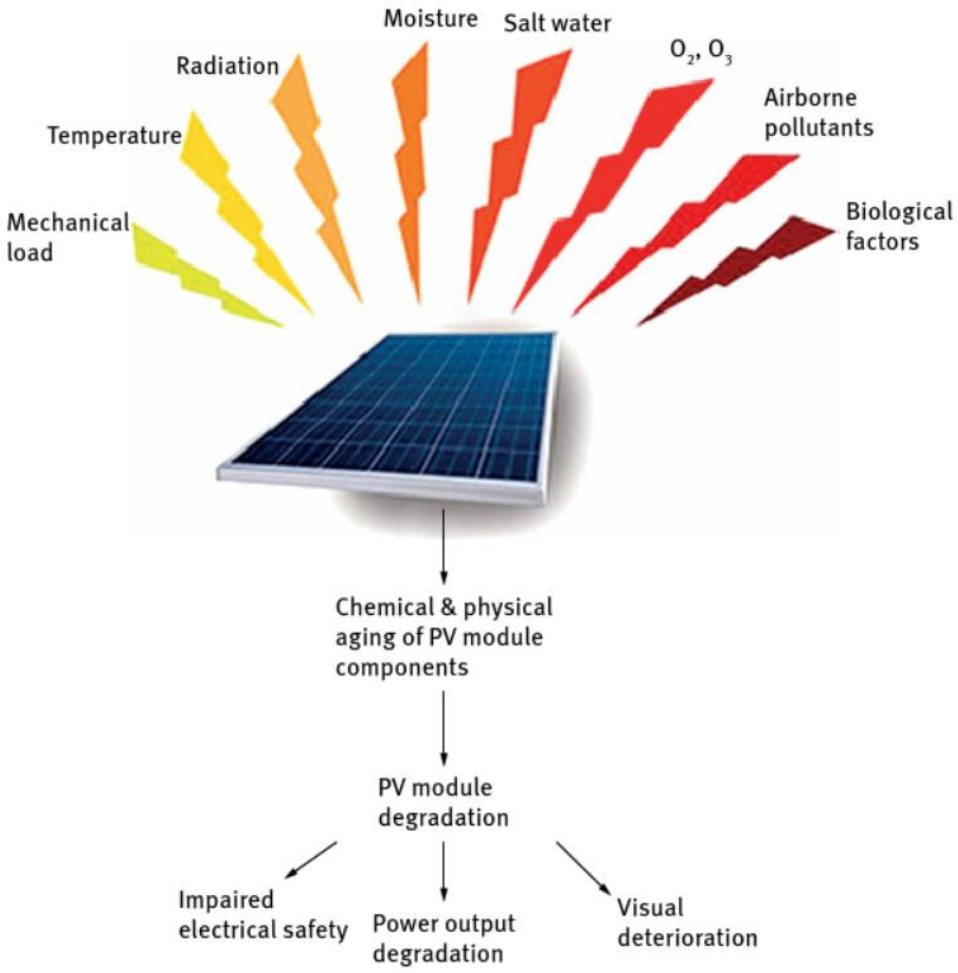

Figure 3.1. *External loads impacting PV module performance* ***[14]****.*

3.1 Hot Spots

Hot spots formation within the PV modules results from localized heating conditions, which can be caused by partial shading conditions, mismatched PV cells, and internal PV cell defects. Consequently, hot spots can lead to performance degradation of the PV modules over the long-term, damage of the modules, and it may cause a serious safety risk for the PV system and the operators [15].

Hot spots occur when series-connected PV cells are exposed to non-uniform irradiance levels. In this case, the non-shaded PV cells produce a higher current and push it through the affected PV cells. Thus, the shaded PV cell is subjected to high reverse voltage, which is limited by the breakdown voltage of the p-n junction. The shaded PV cell then acts as a load, absorbs power instead of generates it, which may lead to permanent damage when the absorbed power exceeds the critical power dissipation of the PV cell. The hot spot formation in series-connected PV cells is illustrated in figure 3.2 [5] [16].

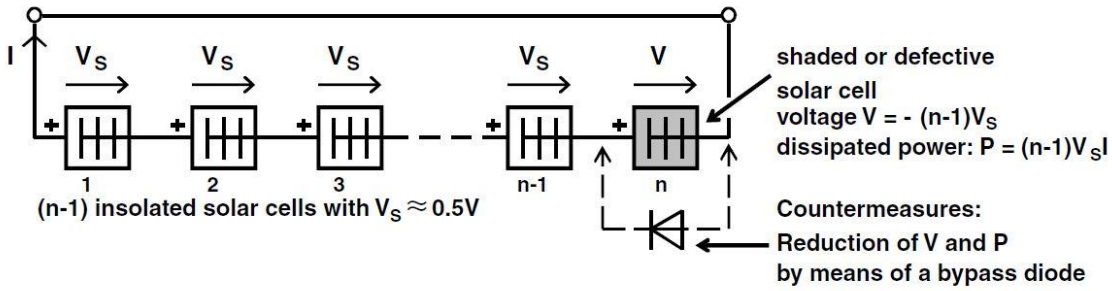

Figure 3.2. *Series-connected PV cells during partial shading* ***[5]****.*

Bypass diodes are usually used in PV modules to eliminate hot spots formation. These diodes are connected in antiparallel to series-connected PV cells. Furthermore, depending on the PV module manufacturers, one bypass diode may be connected in parallel with a 12-24 group of series-connected PV cells. When a PV cell is locally shaded in a group of series-connected PV cells, an alternative path for the current produced by other groups of PV cells is provided by a bypass diode. However, in some specific conditions hot spots may still happen specially when the shading is not extremely high. This can happen due to nonhomogeneous dust accumulation on the healthy PV modules, which doesn't not activate bypass didoes.

Figure 3.3 shows a bypass diode connection with a group consists of 12 series-connected PV cells.

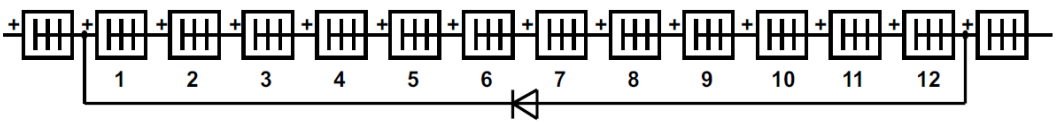

Figure 3.3. *Bypass diode connection with a group of series-connected PV cells* ***[5]****.*

Figure 3.4 shows *a* PV module under partial shading caused by a shrub. The thermography image shows a hot-spot formation in the PV module with a reference temperature of 38.7 ℃ whereas the temperature of the shaded PV cell was raised to 50.4 ℃ [5].

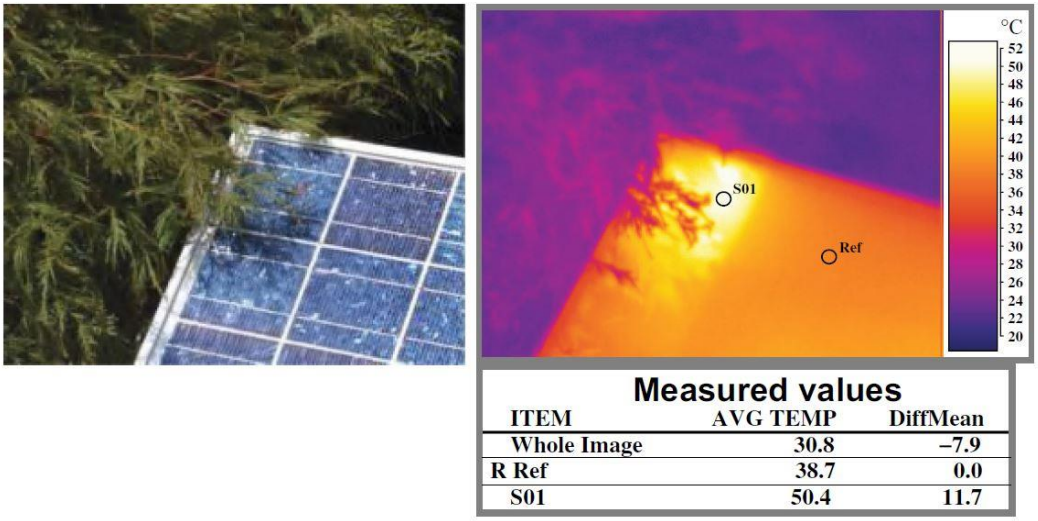

Figure 3.4. *Hot-spot formation in the PV module under partial shading* ***[5]****.*

3.2 Photovoltaic Cells Cracks

PV cells cracks can arise during the wafering process, PV cell/module production, transportation, and installation phases. Cell cracking can impact the reliability of the PV modules over the long-term and it may lead to reduction in the power output. However, cell cracking may cause a significant impact on the power production of the PV modules under real operating conditions as modules are subjected to different environmental effects such as humidity, thermal stress, and mechanical loads. Furthermore, the power loss caused by the cell cracks develops with time and lastly may lead to electrical disconnection. As wafer thickness is decreased, the potential of cell cracks during the production process becomes greater. Cell cracks and inactive areas in the PV module can be detected effectively by Electroluminescence (EL) imaging technique. Commonly, PV modules manufacturers utilize automated EL imaging techniques with software to detect the cell cracks in the production line. Based on the internal criteria of the manufacturer, PV modules might be rejected depending on the number of cracks in the cell and the number of the cracked PV cells in the module. Figure 3.5 shows various shapes for PV cell cracks [17].

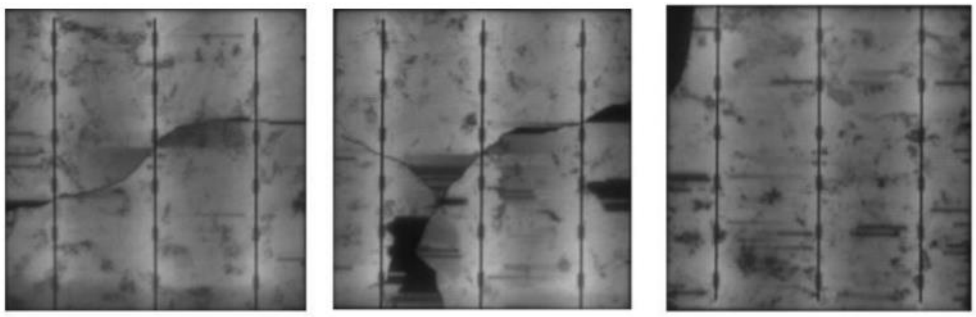

Figure 3.5. *PV cell cracks with different shapes* ***[17]****.*

3.3 Snail trails

In the last few decades, the snail trails phenomenon (also named snail tracks) has been observed on the front side of some crystalline silicon PV modules within a certain time after the installation. Snail trail has been identified as a discoloration defect in the PV modules. In addition, it may appear on different types of PV cells, such as monocrystalline and polycrystalline solar cells. This defect indicates discolored silver fingers, which appear as small dark lines on the surface or the edge of the PV cells. Snail trails within the PV cells can be highly associated with micro-cracks which can be considered a pre-

requisite for the appearance of snail trails. Furthermore, the investigations by many researchers showed that the snail trails formation might also be correlated with humidity which reacts with the polymer material of the PV modules. Thus, the humidity may spread out through the back sheet inside the PV module. Therefore, a chemical reaction between the front layer of EVA and the silver contact fingers may cause the discoloration of the grid fingers. Figure 3.6 shows two polycrystalline PV modules influenced by snail trails [18] [19].

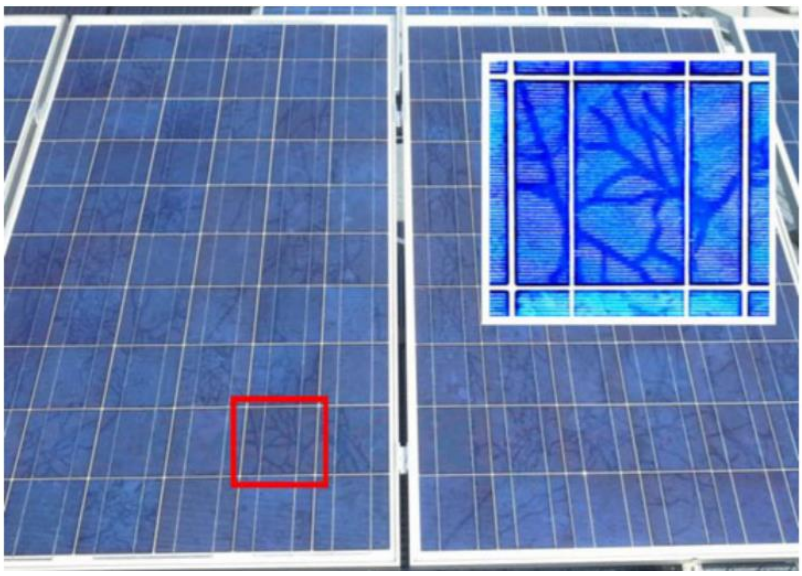

Figure 3.6. *Polycrystalline PV modules affected by snail trails* ***[18]****.*

3.4 Ethylene-vinyl acetate discoloration

Ethylene-vinyl acetate (EVA) is one of the commonly used material for the encapsulation of the PV modules. Discoloration of Ethylene-vinyl acetate (EVA) is one of the main reasons that cause power degradation of aged PV modules. It decreases the transmittance of incident solar irradiance that reaches the PV cells encapsulated in the module leading to reduce the short-circuit current and the output power of the PV module. EVA degradation and discoloration are correlated with a long period of exposure to ultraviolet radiation (UV), in addition to environmental factors that create stresses, such as temperature and moisture. Therefore, PV modules manufacturers use different additives to diminish these influences, such as ultraviolet absorbers and antioxidants. However, due to erroneous manufacturing processes such as inadequate lamination time or using poor quality raw materials and/or due to inappropriate mix of additives rates, EVA may still degrade over a long-time exposure in the field. Moreover, EVA discoloration does not cause a safety issue unless the discoloration is extreme and localized at a single PV cell, where

it may lead to activating the bypass diode. Figure 3.7 shows EVA discoloration in 25-year-old monocrystalline PV module [20] [21] [22].

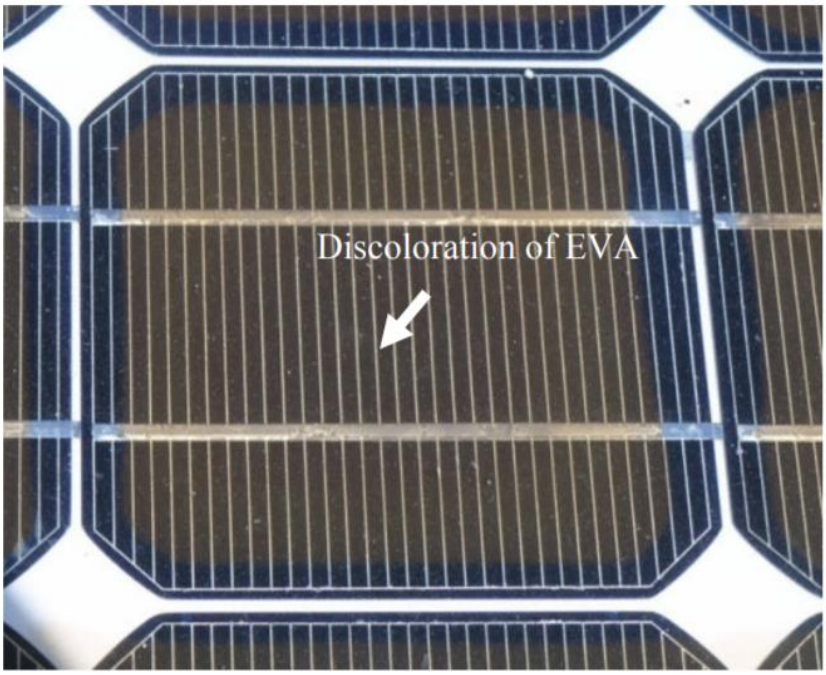

Figure 3.7. *EVA discoloration of aged Monocrystalline PV module* ***[43]****.*

3.5 Delamination

Delamination of EVA encapsulant in PV modules occurs due to the separation between the EVA encapsulant and other layers within the module package. It is one of the most common degradation modes of filed-aged silicon PV modules. Many different types of delamination have been identified in the PV modules in the field. These failures include the delamination of EVA encapsulant at the interface from the front glass of the module, the top surface of the PV cells, interconnect ribbons, and the backsheet of the module. It may be that these failures can cause different impacts on the PV module performance. However, delamination at the interface between encapsulant and the glass has been identified to appear in some PV module types, which manufactured with a non-EVA encapsulant material. The delamination between the EVA encapsulant and the top surface of PV cells is one of the most observed in the field. It is more common that delamination of the EVA encapsulant in the PV modules may happen in the warm and moist climate. However, delamination can lead to performance degradation of the PV modules due to optical decoupling between the EVA encapsulant and the PV cells. The void caused by

the delamination may enable the accumulation of moisture in the PV module. Thus, considerably increasing the possibility of corrosion in the PV cell metallization and can cause a significant reduction in the PV module output power. Figure 3.8 shows PV module failure caused by delamination at the interface between EVA encapsulant and the front side of the PV cells [23] [24].

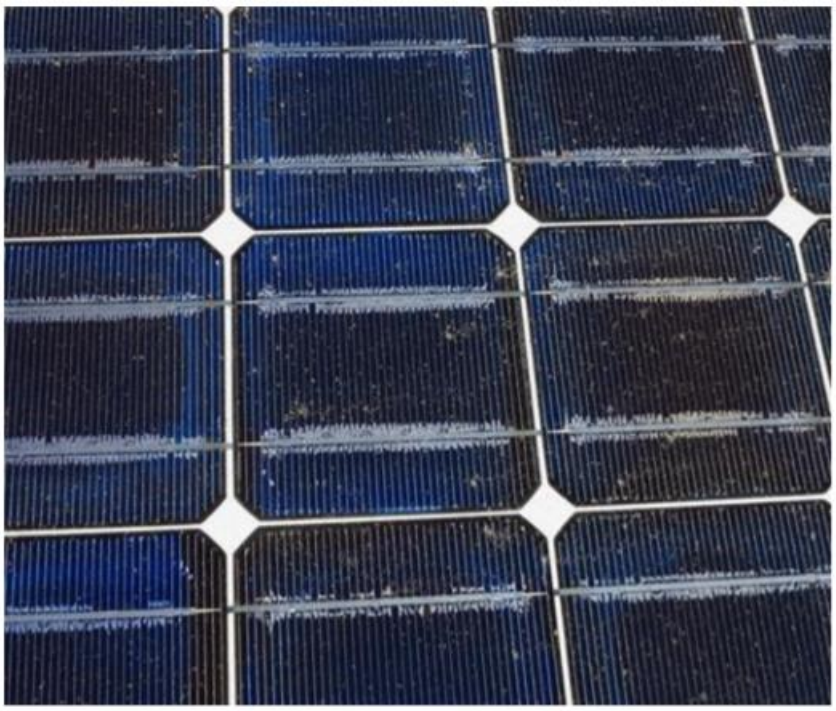

Figure 3.8. *Delamination between encapsulant and the surface of the PV cells in Siemens PV modules* ***[24]****.*

3.6 Broken interconnects

The conventional silicon PV module is composed of multiple individual PV cells. Usually, these cells are interconnected together in series by the interconnect ribbons to increase the PV module voltage. The interconnection ribbon connects the front side with the rear side of the PV cells. These ribbons can be disconnected due to frequent mechanical stress or thermal expansion. Furthermore, poor soldering between PV cell interconnect ribbon and string interconnect in the manufacturing process of PV module is the most common reason for causing disconnections. A short distance between PV cells enhances the breakage of the PV cell interconnect ribbon. However, some of the old PV modules had only one interconnect ribbon for each cell, thus they experienced open circuits when the interconnect ribbon of the PV cell disconnected. Hence, Increasing the

interconnect ribbons was introduced to avoid PV modules failure. Figure 3.9 illustrates an EL image of PV module with several disconnected interconnect ribbons [25] [22].

Figure 3.9. *EL image of PV module with broken interconnect ribbons* ***[25]****.*

4. OVERVIEW OF EXISTING PHOTOVOLTAIC INSPECTION METHODS

PV modules are the main component of the solar PV power plant. During the operation of the solar PV system, the modules might be subject to various defects and failures caused by weather conditions and internal or external stresses. In addition, many failures and faults cause a drop in the output power of the PV system. Moreover, early defects inspection may avoid the degradation of PV modules. Therefore, efficient detection plays a critical role in assuring the lifetime of PV modules, and it is crucially important for PV system operation. Various techniques are applied to diagnose PV modules failures and defects, such as visual inception, PV module I-V curve measurement, Electroluminescence (EL) imaging, UV fluorescence imaging, resonance ultrasonic vibrations, and infrared thermography. Nevertheless, due to the different characteristics of PV modules failures, only some of these methods are reliable and practically applicable. In addition, some of the previously mentioned inspection tools are used to identify specific PV module defects and are not helpful for diagnosis other defects. Due to its fast process and cost-effectiveness, infrared thermotropy has become one of the widely used methods for PV inspection. Furthermore, this technique can precisely locate most defects and failures of PV modules [26].

In this chapter, various inspection, PV module I-V curve measurement, electroluminescence, and IR thermography are discussed.

4.1 Visual Inspection

PV modules performance over the long-term can be dramatically influenced by defects and failures happening fundamentally under real operating conditions. Generally, visual inspection is the first stage and direct method to identify and evaluate PV modules defects and failures. Furthermore, it provides a general overview of the condition of the PV system. In this method, almost all the external stresses on PV modules may be observed. Visible defects such as bubbles, discoloration of EVA encapsulant, delamination, burn marks, PV module glass breakage, cracked PV cells, frame bending, corrosion, scratches, as well as soiling accumulation are detectable by visual inspection. In the following step, a decision about further detection and needed procedure may be taken by the operator of the PV system [27] [28].

4.2 Photovoltaic module current-voltage curve measurement

The measurements of the PV module current-voltage *(I-V)* characteristic curve define the short-circuit current and the open-circuit voltage. The main parameters of the PV module such as the rated maximum power $(P_{\max})$, the voltage and the current at the maximum power point (V_{mpp}) and (I_{mpp}), and the fill factor (*FF*) are extracted from the *I-V* curve. The extracted data is used to assess the quality of the PV module. A portable *I-V* tracer is usually used to measure the *I-V* curve of the PV module under real sunlight conditions. Furthermore, the traditional method of detecting the failures and defects in the PV modules by using electrical characteristic measurements is a well-known method. This technique has limited capability for identify PV modules defects and failures. Indeed, an anomalous in the *I-V* characteristic curve or a decreased power output of a PV power system might refer to an existing failure in the system. However, it is difficult to detect the precise physical fault position in this method without carrying out further electrical measurements to each PV module individually. Furthermore, it is obvious that such a method is expensive, time-consuming, and may not be practically efficient or agreeable by PV systems operators. Figure 4.1 shows multifunction photovoltaic tester device manufactured by Italian company called HT [29] [22] [30].

Figure 4.1. *Multifunction photovoltaic tester device* ***[30]****.*

4.3 Electroluminescence

The electroluminescence imaging (EL) technique is commonly used as an inspection tool for materials and production quality of the PV modules, both in the manufacturing stage and in real operating conditions. EL images can expose comprehensive data on the mechanical integrity of the PV modules. In this technique, the pattern of the defect may help to specify the origin of the defect. These defects can be attributed to the crystallization of silicon or the manufacturing process of the PV cells and modules. Fully dark areas within the PV cell active area in the EL image of the module refer to disconnection of the PV cell metallization. Due to the commercial PV cells are quite thin with large size, the PV cells of modules may break during the manufacturing process, transport, and installation. Conventionally, EL image technology has been utilized by the operation and maintenance (O&M) companies for a qualitative inspection of PV cells cracks in the real operation conditions. In this method, a DC current is applied to the PV modules to energize the radiative recombination in the PV cells, which creates light emission in the PV cells. This released light is detected via an electroluminescence camera, where the light emission density refers to the health status of the PV cells. Figure 4.2 shows EL image of monocrystalline PV module. The EL image of the module shows several cracks which appear as dark areas within the PV cells [31] [32].

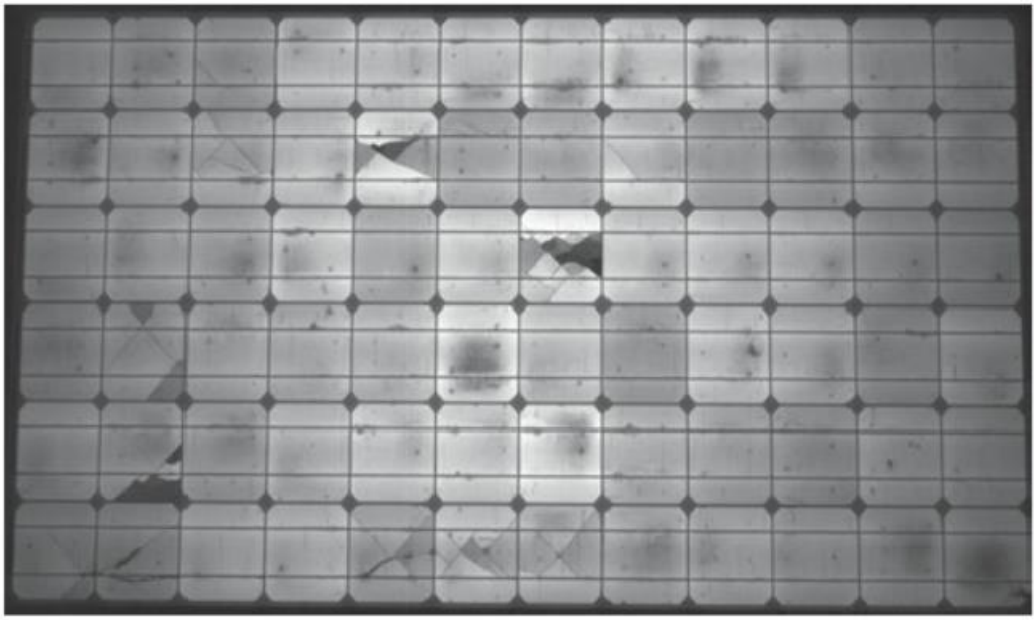

Figure 4.2. *EL image of PV module representing cells cracks* ***[32]****.*

4.4 Infrared thermography

All bodies with temperatures above 0 K (absolute zero) emit energy in the form of electromagnetic waves. The strength of the emitted energy is directly proportional to the temperature of the body. It propagates with the speed of light without a medium. IR thermography cameras acquire infrared radiation emitted by a body and convert it into an electronic signal [33].

As shown in figure 4.3, the infrared radiation (IR) region can be divided based on wavelength into several spectral bands as follows:

- Near-infrared (NIR), $(0.75 - 1\ \mu m)$
- Short wave infrared (SWIR), $(1 - 2.7\ \mu m)$
- Mid wave infrared (MWIR), $(3 - 5\ \mu m)$
- Long wave infrared (LWIR), $(8 - 14\ \mu m)$

Most of the thermographic cameras can detect longwave infrared radiation in the region $(8\mu m - 14\ \mu m)$. Figure 4.3 shows infrared radiation as a subset of the electromagnetic spectrum [34].

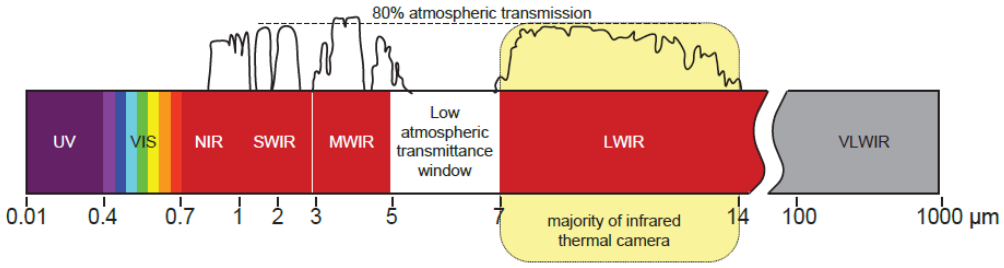

Figure 4.3. *The electromagnetic spectrum, including the infrared radiation bands* ***[34]****.*

Infrared (IR) cameras can be utilized to detect the heat emitted within the PV modules. The camera can identify the temperature differences by detecting the longer wavelength infrared radiation released by the PV modules. Typically, heat dissipation in the PV module refers to a defect or fault that has taken place, either part of PV modules is no anymore generating power at all or due to increasing the resistance to the flow of the current. Thermal camera can be used to inspect the PV systems under real operating conditions. In this technique, the thermal camera can detect the hot spots in the PV modules, defective bypass diodes, and any other faulty components that reach to the phase where they are producing heat and perhaps reducing the output power. One of the main benefits of

using thermal cameras, in this case, is their ability to shoot the images of the modules while the PV system is under actual operation [32].

In recent years, a new application of infrared thermography with unmanned aerial vehicles (UAVs) has been widely used. Aerial thermography (AT) or drone with infrared camera for inspection of photovoltaic (PV) systems has become one of the most promising markets in the solar PV field. Conventionally, faulty PV modules or cells have been detected by applying an electrical measurement test of the I-V curve and/or manual thermography, which present high cost and time-consuming tools [35]. Drones with thermal cameras are a powerful technique for inspection of PV systems, gathering data greater than 50 times faster the manual techniques and enhancing safety [36]. Additionally, drones can take off and land from a particular location, fly large distances, and inspect a big area in a short time. Drones-based thermal cameras reduce the maintenance cost, the work needed, and the data gathered by this tool is very accurate. It can inspect large-scale PV systems and identify faulty PV modules while being in the sky [37]. Figure 4.4 shows drone with thermal camera during the PV system inspection process.

Figure 4.4. *PV system inspection using drone with thermal camera* ***[36]****.*

DJI is one of leader drone manufacturer which capture about 70% of the drone market. The company provides a range of solutions that can be used for the inspection of PV systems. One of these solutions is DJI M300 RTK which can be combined with Zenmuse H20T thermal camera. The commercial drone offers a range of features and capabilities that make it a suitable option for the inspection of PV power plants. The maximum flight time of the drome is 43 minutes with Zenmuse H20T thermal camera, which enables more data collection over a single flight. In addition, the drone comes with hot-swappable

batteries which enables the drone operator to switch them without shutting down the drone. Figure 4.5 shows the MATRICE 300 RTK model of DJI.

Figure 4.5. *DJI MATRICE 300 RTK* ***[36]****.*

DJI Mavic 2 Enterprise Advanced is another solution that can be used for solar PV inspection. This drone is powerful, lightweight, foldable, and it can capture both visible and thermal data. Figure 4.6 displays DJI Mavic Enterprise Advanced [36].

Figure 2.6. *DJI Mavic Enterprise Advanced* ***[36]****.*

5. ANALYSIS AND RESULTS

The main objective of this chapter is to introduce and familiarize the reader with the approach used to detect the defects and failures of the PV modules in Tampere University solar PV power research station. First, the drone that has been used in this investigation is presented. DJI Mavic 2 Enterprise Dual specifications and features are briefly illustrated in this chapter. After that, the solar PV research power station at Tampere is shortly described. Next, the experiment procedures and implementation of the flight mission are illustrated. In the last part of this chapter, the experiment results which include the study cases and analysis are discussed in detail.

5.1 Drone-based infrared thermography

The measurements in this work were carried out with DJI Mavic 2 Enterprise Dual. The drone is manufactured by a drone company called DJI.

5.1.1 The drone specifications and features

The DJI Mavic 2 Enterprise Dual offers a fully stabilized gimbal camera on 3-axis, enabling the drone user to shoot clear images and stable videos. The drone has a long-wavelength infrared thermal camera and RGB camera, providing at the same time both infrared and visible imaging. In addition, the drone comes with 24 GB of internal memory to store the captured images and videos. Moreover, a micro-SD card can be attached to the drone for storing the images and videos. DJI Mavic 2 Enterprise Dual has an infrared camera with a resolution of (120×160) pixels. The visual camera shoots 4K videos and 12-mega pixel images. DJI remote controller is integrated with $\mathrm{OcuSync}^{\mathrm{TM}}$ 2.0 long-range wireless transmission technology, providing a maximum transmission range of 10 km and presenting a live video from the drone to the DJI smart controller screen. The drone and its gimbal camera can be controlled simply via the joysticks of the remote controller. Furthermore, DJI remote controller LCD screen displays real-time drone information. The removable joysticks make the remote controller not difficult store. The maximum flight speed of DJI Mavic 2 Enterprise Dual is 72 km/h with 31 minutes as maximum flight time. DJI Mavic 2 Enterprise Dual supports Return to Home (RTH) safety feature which is activated by tapping and holding the RTH button on the flight controller. This function brings the drone back to the home point when the drone battery is depleted. The drone

weight without accessories is 899 g. The drone includes an intelligent flight battery having a 15.4 V, 3850 mAh LiPo type battery with a smart charger [38]. Figure 5.1 shows DJI Mavic 2 Enterprise dual that has been used in this investigation. Tables 5.1 and 5.2 represent the technical specifications of the drone thermal and visual cameras, respectively [39].

Figure 5.1. *DJI Mavic 2 Enterprise Dual its visual and thermal cameras, flight controller, battery charger, and additional accessories.*

Table 5.1 technical specifications of DJI Mavic 2 Dual Enterprise thermal camera [39].

Sensor	Uncooled VOx Microbolometer
Lens	HFOV: 57° Aperture: f/1.1
Sensor Resolution	160×120
Pixel Pitch	12 µm
Spectral Band	8-14 µm
Image Size [2]	640×480 (4:3); 640×360 (16:9)
Still Photography Modes	Single shot Burst shooting: 3/5/7 frames
Video Recording Modes	640×360 @8.7fps
Accuracy	High Gain: Max ±5% (typical) Low Gain: Max ±10% (typical)
Scene Range	High Gain: -10° to +140°C Low Gain: -10°to +400°C
Photo	JPEG
Video	MP4, MOV (MPEG-4 AVC/H.264)

Table 5.2 technical specifications of DJI Mavic 2 Enterprise Dual visual camera ***[39]***.

Sensor	1/2.3" CMOS; Effective pixels: 12M
Lens	FOV: approx. 85° 35 mm format equivalent:24 mm Aperture: f/2.8 Focus: 0.5 m to ∞
ISO Range	Video: 100-12800 (auto) Photo: 100-1600 (auto)
Max Image Size	4056×3040 (4:3) ; 4056×2280 (16:9)
Still Photography Modes	Single shot Burst shooting: 3/5/7 frames Interval (2/3/5/7/10/15/20/30/60 s)
Video Recording Modes	4K Ultra HD: 3840×2160 30p 2.7K: 2688×1512 30p FHD: 1920×1080 30p
Max Video Bitrate	100 Mbps
Photo	JPEG
Video Format	MP4, MOV (MPEG-4 AVC/H.264)

5.1.2 Preparing for the flight mission

In Finland, flying a drone for commercial operation is subjected to European drone' regulation. The regulation is observed and implemented by The Finnish Transport Safety Agency (Trafi). According to the regulation, drone users must register as drone operators. Additionally, drone users must take and pass an online theoretical test before flying and operating the drone [40]. To perform this work, the registration procedures have been done in cooperation with Cleaner Future Oy and the online exam is passed. Figure 5.2 shows the completion certificate of the online training organized by Trafi, which allows the operator to fly the drone.

Figure 5.2. *Proof of completion of the online training.*

5.2 Tampere University Photovoltaic Power Research Station

The Tampere University solar PV power research station was built in the year 2010 on the rooftop of the Department of Electrical Energy Engineering. The total installed capacity of the PV power research station is 13.1 KWp with 69 NP190GKg PV modules manufactured by a Finnish company called NAPS Solar Systems Oy. The PV module in this system is comprised of 54 series-connected polycrystalline silicon PV cells and contains three bypass diodes. Each bypass diode is connected in parallel with a group of 18 PV cells. The solar PV power station was designed to be a grid-connected PV system for research objectives. Figure 5.3 displays an aerial image taken by DJI Mavic 2 Enterprise Dual for part of the solar PV power research station. The electrical specifications and physical dimensions of the NP190GKg PV module are listed in table 5.3 [9] [41] [11].

Figure 5.3. *Arial image for Part of Tampere University Solar PV power plant.*

Table 5.3 *Electrical specification of the NP190GKg PV module under STC* ***[42]****.*

Power at max power point (P_{MPP})	190 W
I_{MPP}	7.33 A
V_{MPP}	25.9 V
I_{SC}	8.02 A
V_{OC}	33.1 V
Dimensions (length, width, thickness)	1475 mm x 986 mm x 35 mm
Weight	19.5 kg

Figure 5.4 illustrates the *I-V* and *P-V* characteristic curves of the NP190GKg PV module under standard test condition (STC) [42].

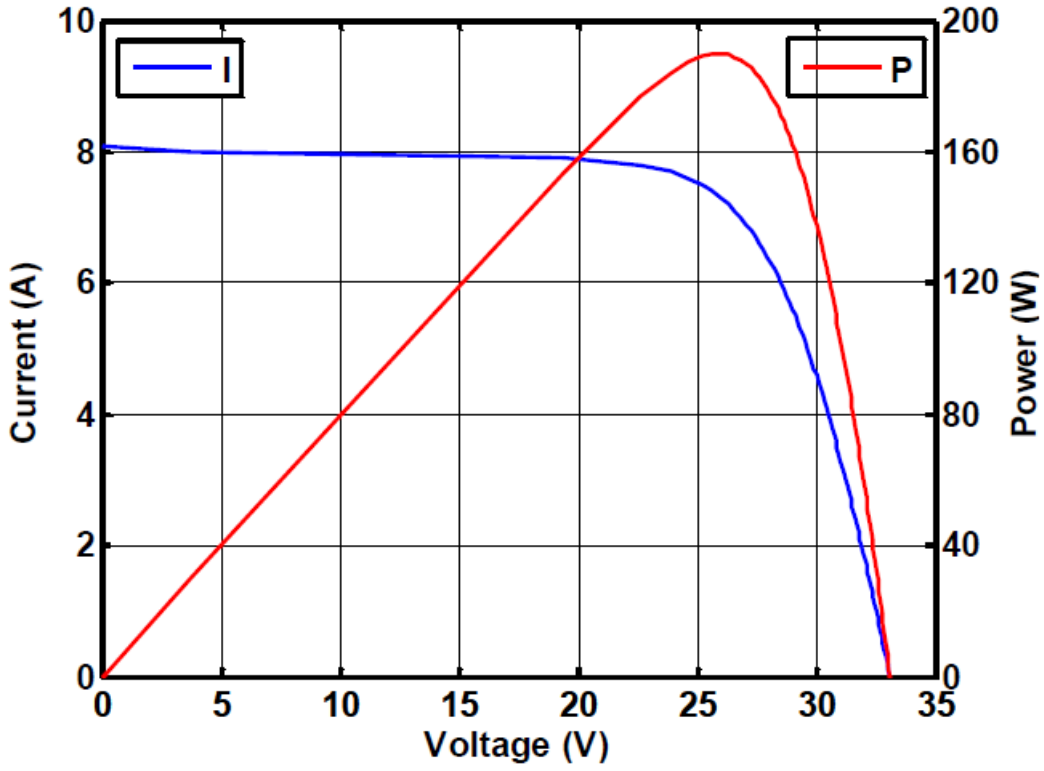

Figure 5.4. *I-V and P-V characteristics curves of the PV module under STC* ***[42]****.*

5.3 Implementing the flight mission

The experiment was implemented on Tampere University solar PV research power station over two days, on 12th and 13th of May 2021. To perform usable aerial thermal data, the measurements were conducted on calm, sunny, clear sky days between 10:00 and 14:00. The weather data during the flight time are obtained from Tampere University photovoltaic station weather data as follows:

- The global solar radiation values were varied between $600\ \mathrm{W/m^2}$ and $700\ \mathrm{W/m^2}$
- The ambient temperature was $24\ ℃$.
- Humidity was 0.2%.
- The wind speed was 6 m/s.

In this investigation the drone was set to fly manually, without planning a specific automatic flight route. The flight altitude was at around 6m above the PV modules. As an initial step, the drone camera has been set on thermal (IR) mode. The temperature range of the thermal camera has been adjusted to be within the range from 20 to 70 ℃. The drone battery was charged up fully before the flight mission. The angle of view (AOV) of the thermal camera has been adjusted as closely as possible to 90^0 with the plane of the PV modules where the reflectivity and emissivity of the surface of the module are respectively at the smallest and greatest level at 90^0. In this experiment, the visual and thermal images were captured and saved, simultaneously. The captured visual images have been used for the general perspective of the solar PV power research station. The thermal images have been employed to observe the variations in temperature homogeneity of the PV modules due to the possible failures and defects. The captured visual and thermal images were saved in an internal drone SD card, then transformed via Bluetooth to the laptop for further analysis. Figure 5.5 shows an aerial visual imagery of the string 2 taken by DJI Mavic 2 Enterprise Dual. The drone flight time duration in this experiment was took about 5 minutes, but the measurements was repeated many times over two days.

Figure 5.5. *Visual image taken by DJI Mavic 2 Enterprise dual for the string 2.*

5.4 Case 1, defective photovoltaic cell

Figures 5.6 and 5.7 show aerial visual and thermal images for the leftmost PV modules of string 2, respectively. These images were captured during the inspection procedure by DJI Mavic 2 Enterprise Dual over the solar PV research power station. As can be observed in figure 5.7, the thermal image shows an overheated PV cell in the leftmost PV module of the string 2. In addition, the thermal image shows the two other adjacent PV modules in healthy condition.

Figure 5.6. *Visual image of the leftmost modules of the string 2.*

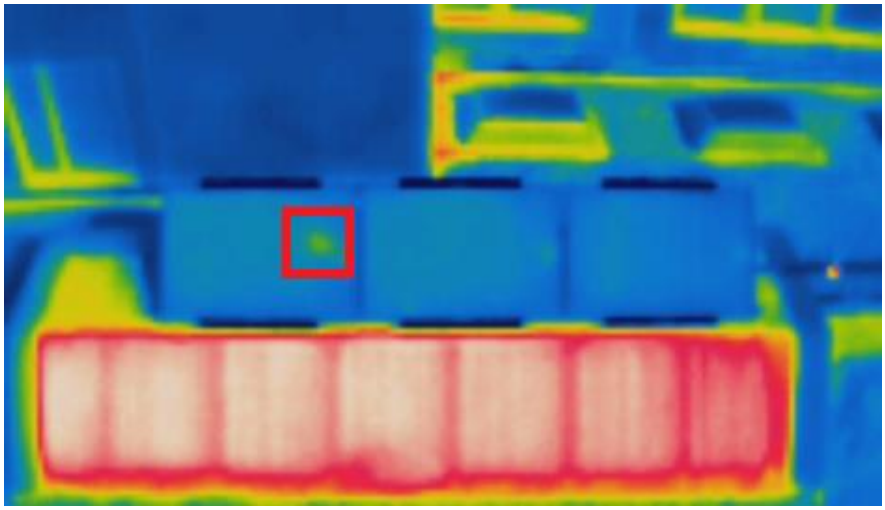

Figure 5.7. *Thermal image of the leftmost modules of the string 2 with overheated PV cell.*

As can be seen in figure 5.8, the thermal image of the leftmost PV module shows a hot-spotted PV cell having an area with a temperature reaching 49.9 ℃. However, this defective PV cell emits higher temperature than the healthy PV cells by several degrees. Furthermore, for a long period of time the defective PV cell has the capability to burn through its back encapsulation.

.

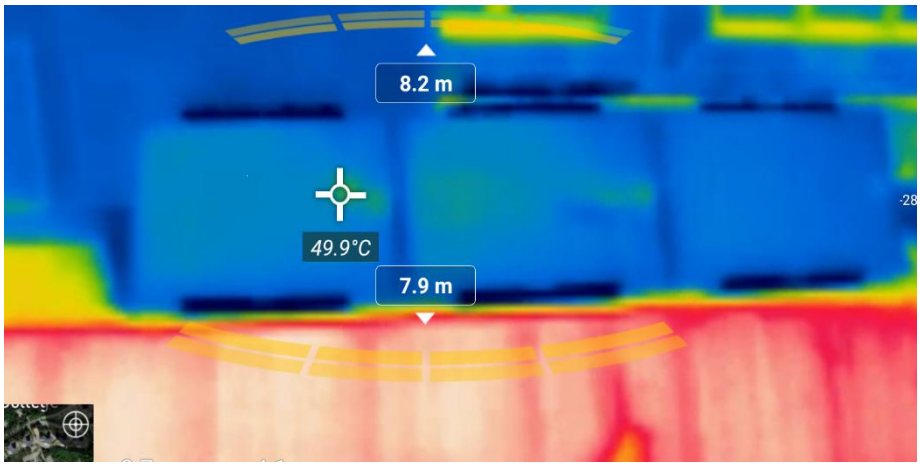

Figure 5.8. *Thermal image of the leftmost modules presenting temperature measurement of the hot spotted PV cell.*

This individual defective PV cell is overheated due to an internal problem, which might be a bad soldering or broken PV cell, as figure 5.9 indicates. The PV module consists of a group of PV cells connected, which are not running at individual maximum power points, but they operate as combined maximum power. Therefore, the hot-spotted PV cell has a direct impact on the PV module operation and performance. Consequently, it will lead to a decrease in the output power of the PV module.

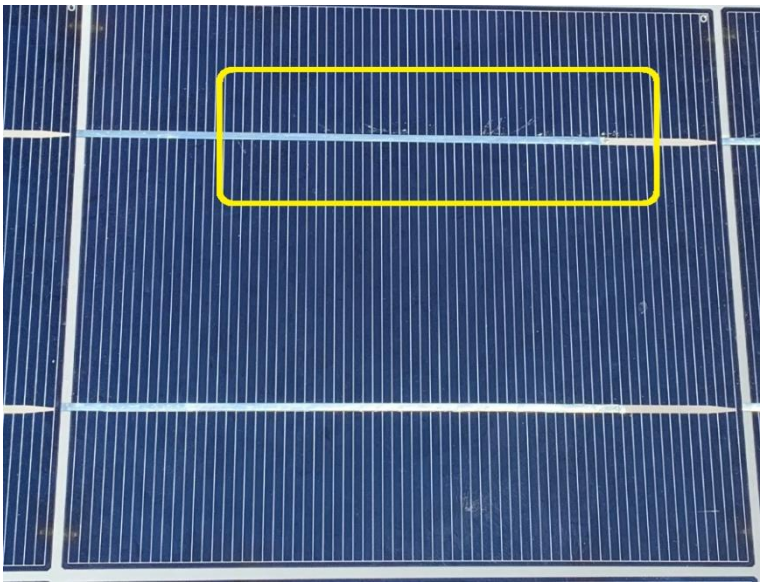

Figure 5.9. *PV cell internal problem within the leftmost PV module of the string 2.*

DJI Mavic 2 Enterprise Dual allows the specified temperature domain to be represented with various color patterns, so that the targets measured appear with higher contrast and more improved visibility. Figure 5.10 shows IR image with different color pattern for the leftmost PV modules of the string 2.

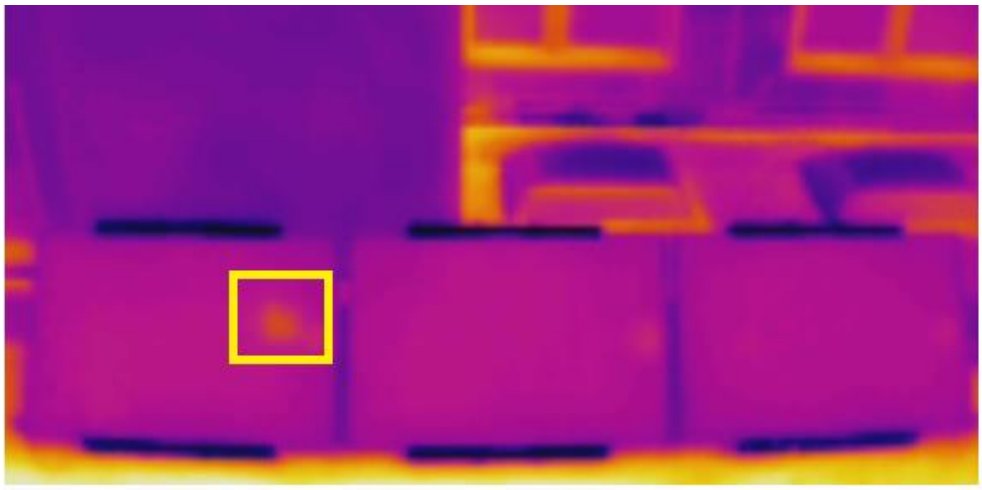

Figure 5.10. *IR image of the leftmost PV module of the string 2 represented with another color pattern.*

5.5 Case 2, an artificial shadow on two adjacent photovoltaic cells

As shown in figure 5.11, an artificial partial shadow was applied on one of the PV modules belonging to the string 2 by covering two adjacent PV cells. The artificial shadow was created by using plastic rod with a small piece of carton. The PV modules of the string 2 have a height of 1 m above the ground. Thus, the plastic rod was fixed on a ladder to make the artificial shadow on the cells possible. In this investigation, the artificial shadow was placed at distance of 1 meter from the PV modules. The main goal of the case study is to explore the shadow effect on PV cells by comparing the hot-spotted PV cells temperature with the temperature of the healthy cells.

Figure 5.11. *an artificial partial shadow on two adjacent PV cells.*

Figures 5.12 and 5.13, respectively, show the visual and thermal images of the artificial shadow on two adjacent PV cells.

Figure 5.12. *Visual image of an artificial shadow on two contiguous PV cells.*

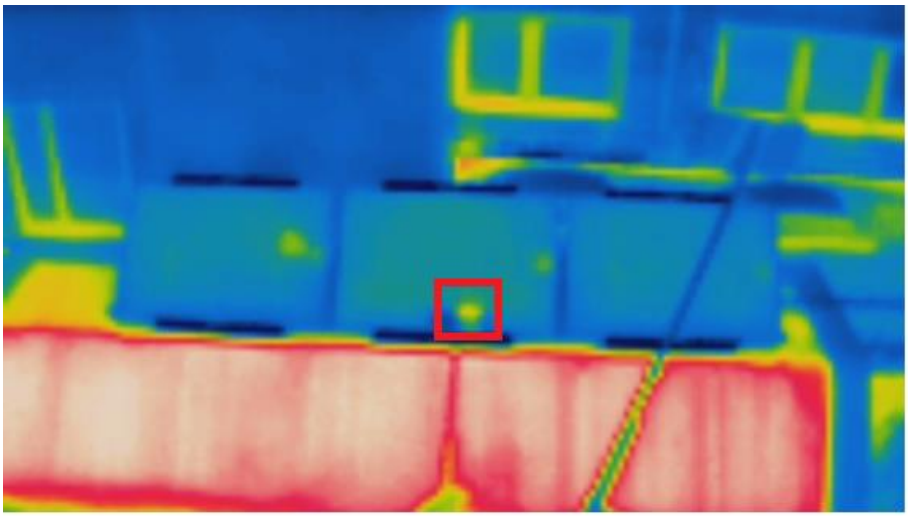

Figure 5.13. *Thermal image with hot spot due to an artificial shadow on two adjacent PV cells.*

As can be seen in figure 5.13, the thermal image shows hot spot area due to artificial shadow applied on two nearby PV cells. The shaded PV cells consume the generated electric power by other PV cells protected by one bypass diode. Furthermore, the thermal image shows the area of two shaded PV cells with darker yellow color refers to higher temperature gradient than one defective PV cell case.

As can observed in figure 5.14 which shows IR image with another color scheme, the two hot-spotted PV cells having temperature reaching 55 ℃ .

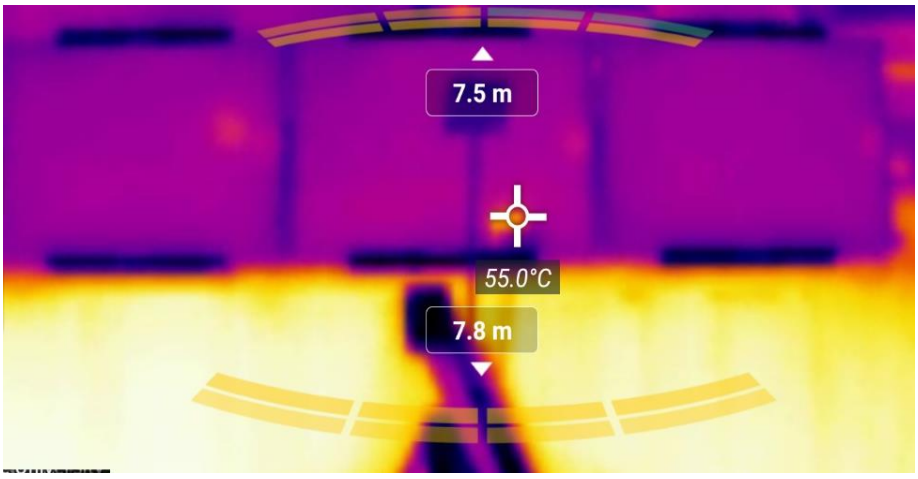

Figure 5.14. *Thermal image with the temperature measurement of the hot spotted PV cells.*

The expected PV cell operating temperature T_{Cell} can be calculated as follows:

$$T_{\mathrm{Cell}} = T_{\mathrm{air}} + \frac{\mathrm{NOCT} - 20\ ℃}{800\ \mathrm{W/m^2}}\ \mathrm{S} \tag{4}$$

Where S is the solar radiation level in $\mathrm{W/m^2}$, NOCT is the nominal operating cell temperature in ℃, and T_{air} is the air ambient temperature in ℃.

Nominal operating cell temperature (NOCT) is reported in NAPS NP190Gkg PV module datasheet, which is 46 ℃, solar radiation level S and air temperature T_{air} are determined from the weather data of the specified measurement day.

Since an artificial shadow has been made on two nearby PV cells, therefore, these two shaded PV cells behave as a load, dissipating heat and causing an increase in the temperature of the two PV cells from 43.5 ℃ to 55 ℃.

5.6 Case study 3, overheating the junction box of the module

The thermographic image of the leftmost modules of the string 2 is presented in figure 5.15. As can be seen in figure 5.15, the junction box area of the PV module is slightly hotter than the rest of the PV module. The reason behind that situation is because the junction box behind the PV module inhibits the cooling down of the PV module a little bit in that area. However, sometimes heating of the junction box of the PV module may refer to thermal abnormalities case, too.

To minimize the hot spot effects, a bypass diode is connected in antiparallel with a group of series connected PV cells is called string. When the PV cells are normally operating, bypass diodes are in revere biased condition and hence inactive. However, because of partial shading or the mismatch between the PV cells, the bypass diodes become forward biased, acting as active, thereby providing an alternative path for the current flow through it. Therefore, the temperature of the active diode is higher than the diode when it is inactive.

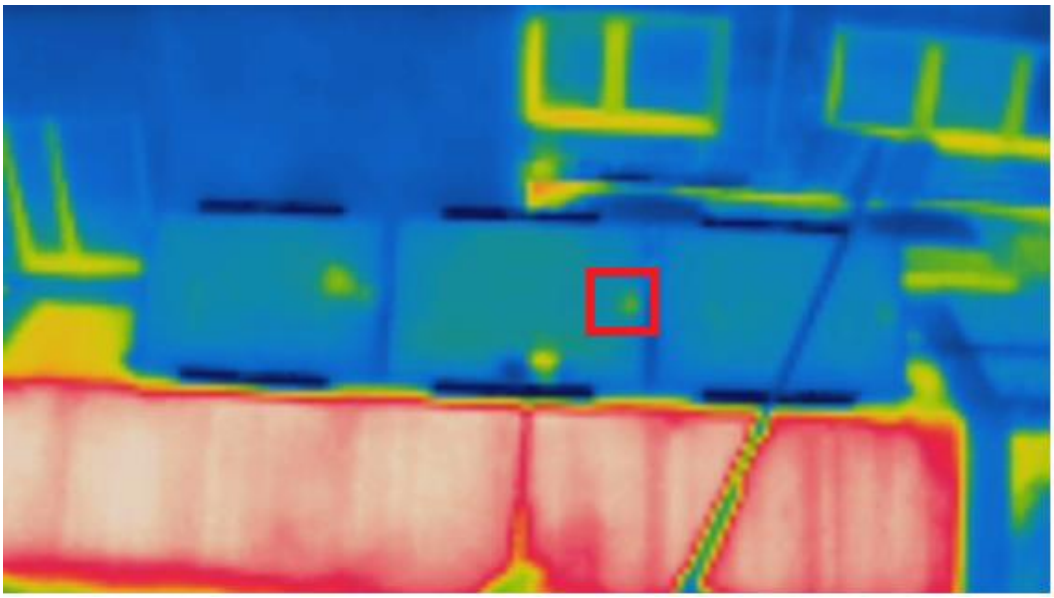

Figure 5.15. *Thermal image with overheated junction box of the module.*

5.7 Case study 4, discoloration of ethylene-vinyl acetate encapsulant

The main target in this thesis was to perform the measurements on the string 2, where it was connected to the power grid for that purpose. However, the thermal inspection has been executed for the uppermost rooftop PV modules of Tampere University PV power station. These modules are not connected to the power grid or an external load. In addition, each of these PV modules is disconnected by a switch. Thus, the PV modules of the front row are in open circuit condition. Figure 5.16 shows an RGB image for the PV modules of the uppermost rooftop of the building.

Figure 5.16. *RGB image of the uppermost rooftop PV modules of the Tampere University PV power station.*

A severe hot-spotted PV cell was detected in the leftmost PV module of the first row of the uppermost rooftop as IR image shows in the figure 5.17.

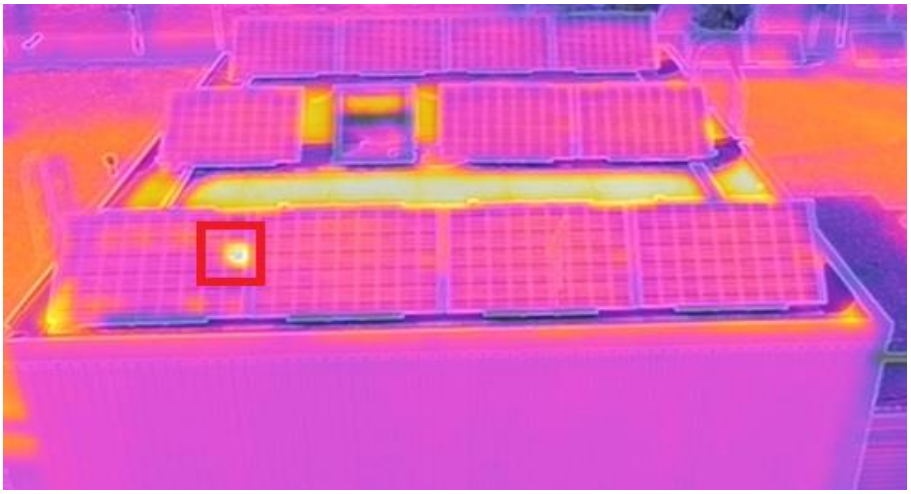

Figure 5.17. *Thermal image with hot spot in the leftmost PV module of the uppermost rooftop.*

Thermal image with another color pattern has been taken as figure 5.18 shows.

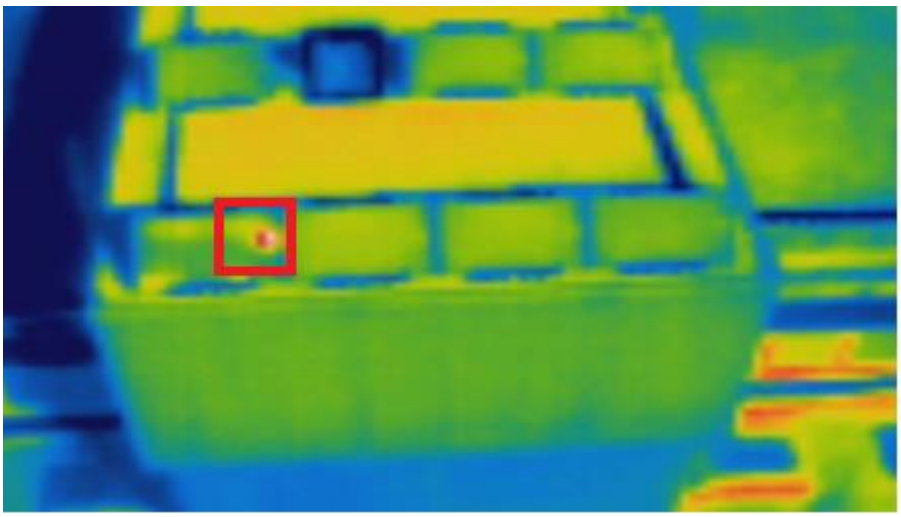

Figure 5.18. *IR image of the uppermost rooftop PV modules with another color pattern.*

As observed in figure 5.19, a significant increase in the temperature of the defective PV cell is found, with temperature of $70.5\ \mathrm{C}^{0}$.

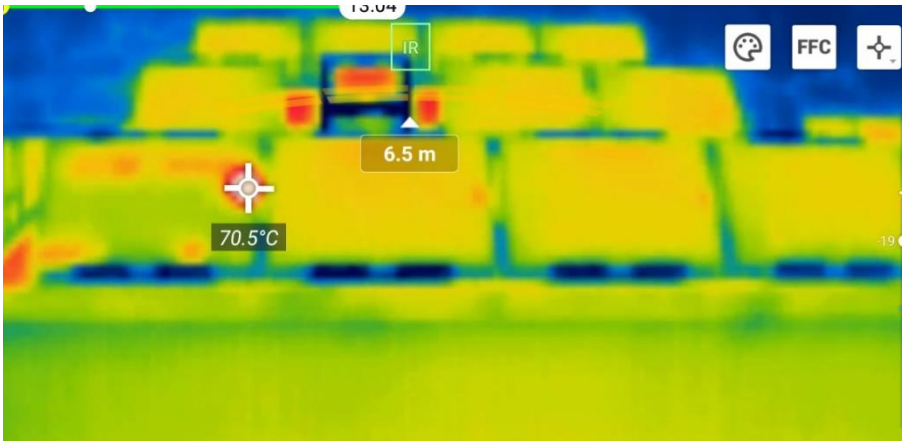

Figure 5.19. *Temperature measurement of hot spot due to EVA discoloration.*

After the measurements has been completed, the leftmost PV module condition has been investigated, it is found that the leftmost PV module on the uppermost rooftop is not open-circuited, but it is short-circuited as shown in the figure 5.20. The other three PV modules on the row are open-circuited.

Figure 5.20. *Leftmost PV module of the first row in short circuit condition.*

As can be seen in figure 5.21, a dark brown area is found in a single PV cell in the leftmost PV module of the uppermost rooftop of the building. This dark brown area is the main cause for the increase in the PV cell temperature. In addition, due to the severity of the defect in the PV cell, which covers almost the entire PV cell area, its temperature was raised remarkably. The defective PV cell exhibits extremely higher level of browning due to so called Ethylene Vinyl Acetate (EVA) discoloration. PV cell discoloration can be seen by naked eyes. EVA Discoloration may result from internal factors, such as the use of bad quality polymers in cells assembly, or external ones, such as hot temperature and humidity. Discolored area reduces the quantity of the sunlight penetrating the cells and thus may result in yield losses.

Figure 5.21. *EVA discoloration in a single PV cell.*

5.8 Case study 5, accumulation of soiling on the photovoltaic module

Data of aerial visual images can provide great visible information about the condition of solar PV power plants. With this technique, some visible defects, and failures of the PV modules such as EVA discoloration, corrosion, soiling, bubble, delamination, snail trails, and cell cracks can be detected. However, the resolution of the visual camera and the flight height must be considered in this procedure.

Visual image of uppermost rooftop PV modules shows accumulation of dirt caused by bird droppings on one of the first row of PV modules as shown in figure 5.22.

The power output of the PV module is highly dependent on the level of solar radiation which reaches the surface of the PV cells. However, the accumulation of dirt on the surface of the PV module reduces the solar radiation reaching the PV cells, which may cause losses in the generated power of the PV module. Therefore, it is very important to clean the PV modules periodically.

Figure 5.22. *Visual image of the uppermost rooftop modules with accumulation of soiling.*

6. CONCLUSIONS AND LIMITATIONS

6.1 Conclusions

Over the coming years, global solar PV power capacity is expected to grow dramatically worldwide. Furthermore, thanks to modern solar PV technologies and low generation costs, the growth of solar PV in many countries continued to rely primarily on utility-scale solar PV systems. In these systems, PV modules are the main component that converts sunlight directly into DC power. Typically, large-scale PV systems may include thousands of PV modules. During the operation of the PV system, PV modules might be subjected to different failures and faults due to internal and external stresses. Thus, the consequence of these factors is the degradation of PV module performance and power loss of the output power of the PV system. In addition, PV modules manufacturers usually guarantee a lifetime of 25 years, but it does not ensure that it can be reached without proper and regular maintenance. Therefore, PV systems maintenance and inspection techniques are increasingly needed to extend the lifetime of PV modules and assure the reliability of these systems. However, efficient, and cost-effective inspection methods of PV systems are crucial to ensure their performance for the long term at the maximum level. Various techniques are applied for the detection failures and defects of PV modules, such as I-V curve measurement, Electroluminescence (EL) imaging, fluorescence imaging, and infrared thermography. However, some of the previously mentioned inspection methods can be applied to identify only specific PV module defects. Infrared thermography has become commonly used as an inspection tool in the solar PV field due to its quickness and reliability. In practice, most of the PV modules defects and failures can be reliably detected with this technology. In this stage of development, a drone-based thermal infrared camera has become a convenient inspection technique to identify the precise location of defective PV cells and modules. In this technique, faulty PV modules can be identified, and thermal abnormalities on the solar PV system are recognized through contactless infrared measurement. In addition, the measurements by thermography drones can be performed during the normal operating conditions of the PV system. This technique represents an efficient, time-saving, and cost-effective solution for the inspection of PV systems compared with other traditional inspection methods.

This thesis was carried out in cooperation with Cleaner Future Oy. The company offers a variety of solar PV solutions, including the design and installation of grid-connected

solar PV systems for residential clients, farms, and industries. Cleaner Future Oy cooperates with an electricity company called VÄRE, which offers power purchase agreements (PPA) to clients. The contract includes selling the electricity generated from solar PV systems to the host clients at a fixed price for the specified time. Additionally, VÄRE Oy is responsible for the maintenance and operation of the PV systems during the duration of the PPA contract. Thus, a thermal imaging drone is required as an efficient inspection tool to follow the condition of the PV system. In this respect, this thesis aims to evaluate and examine the use of DJI Mavic 2 Enterprise Dual for detecting PV modules failures and defects.

DJI Mavic 2 Enterprise Dual was used in this investigation. It is manufactured by SZ DJI, which is one of the world's largest drone manufacturers. The drone is integrated with an alert system called AirSense, which is used to help drone pilots to avoid potential collision hazards with nearby aircraft. Additionally, the drone continuously detects the obstacles through its built-in obstacle sensing system, which notifies the drone pilot through the flight controller when obstacles are too close to the drone. Moreover, the drone is equipped with an infrared camera and a visual (RGB) camera, offering both infrared and visible images at one time.

The main objectives of this thesis are to explore and assess the use of thermal imaging drone technology to detect possible PV modules failures and defects at Tampere University solar PV power research station. The total peak power of the solar PV station is 13.1 KWp generated by 69 NP190Gkg PV modules manufactured by Naps Solar Systems Oy. Each PV module includes 54 series-connected polycrystalline silicon PV cells. Part of the solar PV power station, specifically the string 2, was connected to the power grid to conduct thermal measurements. This string is composed of 17 series-connected polycrystalline PV modules. In addition, further investigation has been made on the uppermost rooftop modules of the solar PV station. In this work, DJI Mavic 2 Enterprise Dual was employed to fly over the PV modules of Tampere University solar PV power station and capture images of modules, both in thermal and visible ranges. The measurements were performed in May 2021 on calm, clear sky days at noon. The solar radiation values during this time varied between $600\ \mathrm{W/m^2}$ and $700\ \mathrm{W/m^2}$. Infrared and visible images of the modules were captured, then extracted from DJI remote controller via Bluetooth to the personal laptop for further analysis. In this investigation, the obtained results were included 5 case studies as follows:

- Hot spotted PV cell in the leftmost module of the string 2.

- Hot spotted two PV cells in the second leftmost PV module of the string 2 due to an artificial shadow on two contiguous PV cells.
- Overheating in the junction box of the second leftmost PV module of the string 2.
- Hot spotted PV cell in the leftmost PV module of the uppermost rooftop due to EVA discoloration.
- Accumulation of soiling on one of the uppermost rooftop modules.

In conclusion, Aerial thermography is an appropriate technique to detect PV modules defects and failures through their temperature distribution under real working conditions. In this thesis, the infrared thermography (IRT) using DJI Mavic 2 Enterprise dual were able through its visual and thermal cameras to detect and identify several defects on PV modules of Tampere University solar PV research power station.

6.2 Limitations

The resolution of the thermal drone camera is one of the most important factors which affect the quality of the measurements. Higher thermal camera resolution enables the detection of smaller targets from larger distances with more accurate images. Today, drones with a thermal camera resolution of 640×480 pixels are available on the market. In this study, the thermal drone camera has a resolution of (120×160 pixels), which is insufficient to accomplish the thermal measurements optimally. Thus, due to the low resolution of the thermal drone camera, the drone flight height in this investigation was reduced at a close distance from the PV modules to perform the measurements acceptably.

One of the critically important features of drone thermography is the flight duration, which depends on the drone's battery. Longer drone flight time means a larger area can be inspected without missing the quality of the measurements or increases the time of the inspection mission. In this work, drone flight time was limited to about 4 minutes due to the limited capacity of the drone battery. In addition, the drone has no additional spare batteries, which can allow for the exchange of the discharged battery with a fully charged one. Thus, the drone was required to return to the home point to recharge the battery. The consumed time for recharge the drone battery was about 45 minutes, which might be considered a long charging time.

One of the main disadvantages of DJI Mavic 2 Enterprise Dual is that the thermal data is not stored in the captured images. However, this feature exists in other expensive DJI products such as Zenmuse XT thermal camera. In this work, the only possible way to obtain images with radiometric data was as screenshots of the screen of the remote controller.

Several environmental factors (e.g., weather conditions, solar radiation, high wind speed, reflection, etc.) may impact the aerial inspection of the PV system.

7. REFERENCES

[1] K. Mertens, “Photovoltaics : Fundamentals, Technology, and Practice,” New York, USA, John Wiley & Sons, 2018, p. 370.

[2] M. Schmela, “Global Market Outlook for Solar Power 2021-2025,” SolarPower Europe, July 2021.

[3] J. A. Tsanakas, L. Ha and C. Buerhop, “Faults and infrared thermographic diagnosis in operating c-Si photovoltaic modules: A review of research and future challenges,” *Renewable and Sustainable Energy Reviews,* vol. 62, pp. 695-709, 2016.

[4] M. Cubukcu and A. Akanalci, “Real-time inspection and determination methods of faults on photovoltaic power systems by thermal imaging in Turkey,” *Renewable Energy,* vol. 147, pp. 1231-1238, March 2020.

[5] H. Häberlin, Photovoltaics system design and practice, John Wiley & Sons, UK 2012.

[6] “National Renewable Energy Laboratory (NREL),” 2021. [Online]. Available: https://www.nrel.gov/pv/assets/pdfs/best-research-cell-efficiencies-rev211011.pdf. [Accessed April 2021].

[7] J. Ventre and R. A. Messenger, “Photovoltaic systems engineering,” Boca Raton, CRC Press LLC, 2010, p. 490.

[8] S. Qazi, Standalone Photovoltaic (PV) Systems for Disaster Relief and Remote Areas, Saint Louis: Elsevier, 2016.

[9] D. T. Lobera, “Modeling and Analysis of the Operation of PV Power Generators Under Varying Atmospheric Conditions,” Tampere University of Technology;, 2014.

[10] K. Lappalainen, “Effects of Climate and Environmental Conditions on the Operation of Solar Photovoltaic Generators,” Tampere University of Technology, 2013.

[11] A. Mäki, J. Huusari, K. Lappalainen, T. Suntio and S. Valkealahti, “Operation of TUT Solar PV Power Station Research Plant under Partial Shading Caused by Snow and Buildings,” *International Journal of Photoenergy,* vol. 2013, no. Article ID 837310, p. 13, 2013.

[12] G. Stapleton and S. Neill, “Grid-Connected Solar Electric Systems,” Florence: Routledge, Taylor & Francis Group, 2012, p. 244.

[13] S. Deshpande and N. R. Bhasme, “A review of topologies of inverter for grid connected PV systems,” *2017 Innovations in Power and Advanced Computing Technologies (i-PACT)-Conference Proceedings,* pp. 1-6, 2017.

[14] H. Wirth, K.-A. Weiß and C. Wiesmeier, “Photovoltaic Modules: Technology and Reliability,” Berlin/Boston, De Gruyter, Inc., 2016, p. 224.

[15] P. Bharadwaj and K. Karnataki, “Formation of Hotspots on Healthy PV Modules and Their Effect on Output Performance,” *2018 IEEE 7th World Conference on Photovoltaic Energy Conversion (WCPEC) (A Joint Conference of 45th IEEE PVSC, 28th PVSEC & 34th EU PVSEC),* pp. 0676-0680, June 2018.

[16] G. Petrone, C. A. Ramos-Paja and G. Spagnuolo, “Photovoltaic sources modeling,” Chichester, West Sussex, United Kingdom, John Wiley & Sons, 2017, p. 205.

[17] V. Gade, N. Shiradkar, M. Paggi and J. Opalewski, “Predicting the long term power loss from cell cracks in PV modules,” *2015 IEEE 42nd Photovoltaic Specialist Conference (PVSC),* pp. 1-6, 17 December 2015.

[18] A. Dolara, S. Leva, G. Manzolini and E. Ogliari, “Investigation on Performance Decay on Photovoltaic Modules: Snail Trails and Cell Microcracks,” *IEEE Journal of Photovoltaics,* vol. 4, no. 5, pp. 1204 - 1211, 2014.

[19] S. Richter, M. Werner and C. Hagendorf, “Understanding the Snail Trail Effect in Silicon Solar Modules on Microstructural Scale,” *27th European Photovoltaic Solar Energy Conference and Exhibition,* pp. 3439 - 3441, 2012.

[20] C. Shashwata, S. Chetan, K. Anil, V. Juzer, Sai.Tatapudi and G. TamizhMani, “Quantification of PV Module Discoloration Using Visual Image Analysis,” *2017 IEEE 44th Photovoltaic Specialist Conference (PVSC),* pp. 1850-1854, 2018.

[21] H. A. Mahdi, P. Leahy and A. Morrison, “Predicting Early EVA Degradation in Photovoltaic Modules From Short Circuit Current Measurements,” *IEEE Journal of Photovoltaics ,* vol. 11, no. 5, pp. 1188 - 1196, 21 June 2021.

[22] M. Köntges, S. Kurtz, C. Packard, U. Jahn, K. Berger, K. Kato, T. Friesen, H. Liu and M. Iseghem, “Review of Failures of Photovoltaic Modules,” IEA-PVPS, 2014.

[23] D. Kim, W. Hong, C. Han and N. Park, “The effect of encapsulant delamination on electrical performance of PV module,” *2011 37th IEEE Photovoltaic Specialists Conference,* pp. 001113-001115, 19 April 2012.

[24] P. Hacke, N. Bosco, D. Miller, M. Kempe, S. Kurtz and J. Wohlgemuth, “Assessing the causes of encapsulant delamination in PV modules,” *2016 IEEE 43rd Photovoltaic Specialists Conference (PVSC),* pp. 0248-0254, 21 November 2016.

[25] J. Wohlgemuth, “Photovoltaic module reliability,” New Jersey, John Wiley & Sons, 2020, p. 264.

[26] R. Zich, S. Leva, F. Grimaccia and A. Gandelli, “IR real-time Analyses for PV system monitoring by digital image processing techniques,” *2015 International Conference on Event-based Control, Communication, and Signal Processing (EBCCSP),* pp. 1-6, 26 October 2015.

[27] M. Aghaei, “SOLAR ENERGY ENGINEERING,” 28 September 2020. [Online]. Available: https://www.study-solar.com/blog-article/failures-defects-in-pv-systems-typical-methods-for-detecting-defects-and-failures. [Accessed 15 june 2021].

[28] M. Aghaei, M. Mussetta, S. Leva, F. Grimaccia and P. Quater, “Light Unmanned Aerial Vehicles (UAVs) for Cooperative Inspection of PV Plants,” *IEEE Journal of Photovoltaics ,* vol. 4, no. 4, pp. 1107 - 1113, 10 June 2014.

[29] F. Barruel, D. Ha, A. Plissonnier, G. Vannier and J. Tsanakas, “Fault Diagnosis and Classification of Large-Scale Photovoltaic Plants Through Aerial Orthophoto Thermal Mapping,” *31st European Photovoltaic Solar Energy Conference and Exhibition,* pp. 1-6, September 2015.

[30] HT, “HT Instruments,” [Online]. Available: https://www.ht-instruments.com/en/products/photovoltaic-testers/commissioning-and-maintenance/pv-isotest/. [Accessed 15 10 2021].

[31] S. Tatapudi, G. TamizhMani, H. Hu, J. Oh, S. Chattopadhyay and C. Castañeda, “Field Inspection of PV Modules: Quantitative Determination of Performance Loss due to Cell Cracks using EL Images,” *2017 IEEE 44th Photovoltaic Specialist Conference (PVSC),* pp. 1858-1862, 05 November 2018.

[32] H. Wirth, K.-A. Weiß and C. Wiesmeier, “Photovoltaic Modules: Technology and Reliability,” Berlin/Boston, De Gruyter, Inc, 2016, p. 224.

[33] S. Lamallam, I. Sebari, A. ElKettani and Y. Zefri, “Thermal Infrared and Visual Inspection of Photovoltaic Installations by UAV Photogrammetry—Application Case: Morocco,” *MDPI,* vol. 2(4), pp. 1-24, 23 November 2018.

[34] D. Muštran, M. Primorac, M. Vukobratović and H. Glavaš, “Infrared thermography in inspection of photovoltaic panels,” *2017 International Conference on Smart Systems and Technologies (SST),* pp. 63-68, 14 December 2017.

[35] S. Gallardo-Saavedra, L. Hernández-Callejo and O. Duque-Perez, “Technological review of the instrumentation used in aerial thermographic inspection of photovoltaic plants,” *Renewable and Sustainable Energy Reviews,* vol. 93, pp. 566-579, October 2018.

[36] “heliguy™,” 28 Sep 2020. [Online]. Available: https://www.heliguy.com/blogs/posts/drones-for-solar-panel-inspections. [Accessed 20 10 2021].

[37] M. Shawky, “geodrones,” 13 MARCH 2021. [Online]. Available: https://geodrones.ae/inspect-solar-plants-10-times-faster-and-50-cheaper-using-drones/. [Accessed 25 10 2021].

[38] DJI, “Mavic 2 Enterprise Series - User Manual v1.8,” 13 04 2021. [Online]. Available: https://www.dji.com/fi/downloads/products/mavic-2-enterprise.

[39] DJI, “Mavic 2 Enterprise Series Specs,” [Online]. Available: https://www.dji.com/fi/mavic-2-enterprise/specs. [Accessed 15 6 2021].

[40] Droneinfo, “Registration and theoretical examination,” 30 09 .2021. [Online]. Available: https://droneinfo.fi/en/registration-and-theoretical-examination. [Accessed 4 10 2021].

[41] D. LOBERA, “Measuring Actual Operating Conditions of a Photovoltaic Power Generator,” Tampere University of Technology, Master of Science Thesis , 2010.

[42] S. Valkealahti, Solar Power Systems Course, Tampere Univeristy , 2019.

[43] N. Park and J.-S. Jeong, “Field discoloration analysis and UV/temperature accelerated degradation test of EVA for PV,” *2013 IEEE 39th Photovoltaic Specialists Conference (PVSC),* pp. 3010-3013, 20 February 2014.